



Three-Dimensional Thermal Model of the Costa Rica-Nicaragua Subduction Zone

JUAN CARLOS ROSAS,¹ CLAIRE A. CURRIE,¹ and JIANGHENG HE²

Abstract—The thermal structure of a subduction zone controls many key processes, including subducting plate metamorphism and dehydration, the megathrust earthquake seismogenic zone and volcanic arc magmatism. Here, we present the first three-dimensional (3D), steady-state kinematic-dynamic thermal model for the Costa Rica-Nicaragua subduction zone. The model consists of the subducting Cocos plate, the overriding Caribbean Plate, and a viscous mantle wedge in which flow is driven by interactions with the downgoing slab. The Cocos plate geometry includes along-strike variations in slab dip, which induce along-strike flow in the mantle wedge. Along-strike flow occurs primarily below Costa Rica, with a maximum magnitude of 4 cm/year (~40 % of the convergence rate) for a mantle with a dislocation creep rheology; an isoviscous mantle has lower velocities. Along-margin flow causes temperatures variations of up to 80 °C in the subducting slab and mantle wedge at the volcanic arc and backarc. The 3D effects do not strongly alter the shallow (<35 km) thermal structure of the subduction zone. The models predict that the megathrust seismogenic zone width decreases from ~100 km below Costa Rica to just a few kilometers below Nicaragua; the narrow width in the north is due to hydrothermal cooling of the oceanic plate. These results are in good agreement with previous 2D models and with the rupture area of recent earthquakes. In the models, along-strike mantle flow is induced only by variations in slab dip, with flow directed toward the south where the dip angle is smallest. In contrast, geochemical and seismic observations suggest a northward flow of 6–19 cm/year. We do not observe this in our models, suggesting that northward flow may be driven by additional factors, such as slab rollback or proximity to a slab edge (slab window). Such high velocities may significantly affect the thermal structure, especially at the southern end of the subduction zone. In this area, 3D models that include slab rollback and a slab edge are needed to investigate the mantle structure and dynamics.

Key words: Subduction zones, thermal structure, geodynamics, numerical modeling, Middle America Trench.

1. Introduction

A subduction zone delineates the convergent boundary between tectonic plates, where oceanic lithosphere descends below a less dense oceanic or continental plate (STERN 2002). As an oceanic plate moves away from a mid-ocean ridge, it thickens and its density increases, eventually becoming negatively buoyant and sinking into the deep Earth (CLOOS 1993). It is generally accepted that this gravitational instability is the primary force driving the motion of the tectonic plates (FORSYTH and UYEDA 1975), and therefore it is not surprising that subduction zones are a topic of intense study. Among subduction zones, the Costa Rica-Nicaragua section of the Middle America Trench (MAT) has received particular attention in recent years. Figure 1 shows the configuration of the MAT in Central America, with the Cocos plate subducting beneath the Caribbean Plate. Subduction in this region is associated with the formation of the Central America Volcanic Arc (CARR *et al.* 2004). It is also responsible for earthquakes that occur within both the Cocos plate and the Caribbean plate, as well as megathrust earthquakes that occur on the inclined subduction interface. The most recent megathrust earthquake was the magnitude Mw 7.6 event that occurred on September 5th, 2012 below the Nicoya Peninsula of Costa Rica (PROTTI *et al.* 2014).

Despite the predominantly trench-perpendicular direction of plate convergence, there are numerous observations that suggest significant along-strike changes in the characteristics of this subduction zone. These include variations in the width of the megathrust seismogenic zone (NEWMAN *et al.* 2002; DESHON *et al.* 2006; SCHWARTZ and DESHON 2007; AUDET and SCHWARTZ 2013), variable amounts of hydrothermal circulation in the Cocos plate crust (FISHER *et al.* 2003; HUTNAK *et al.* 2008; HARRIS *et al.*

¹ Department of Physics, University of Alberta, 4-181 Centennial Centre for Interdisciplinary Science, Edmonton, AB, Canada. E-mail: jrosas@ualberta.ca

² Pacific Geoscience Centre, Geological Survey of Canada, 9860 West Saanich Road, Sidney, BC, Canada.

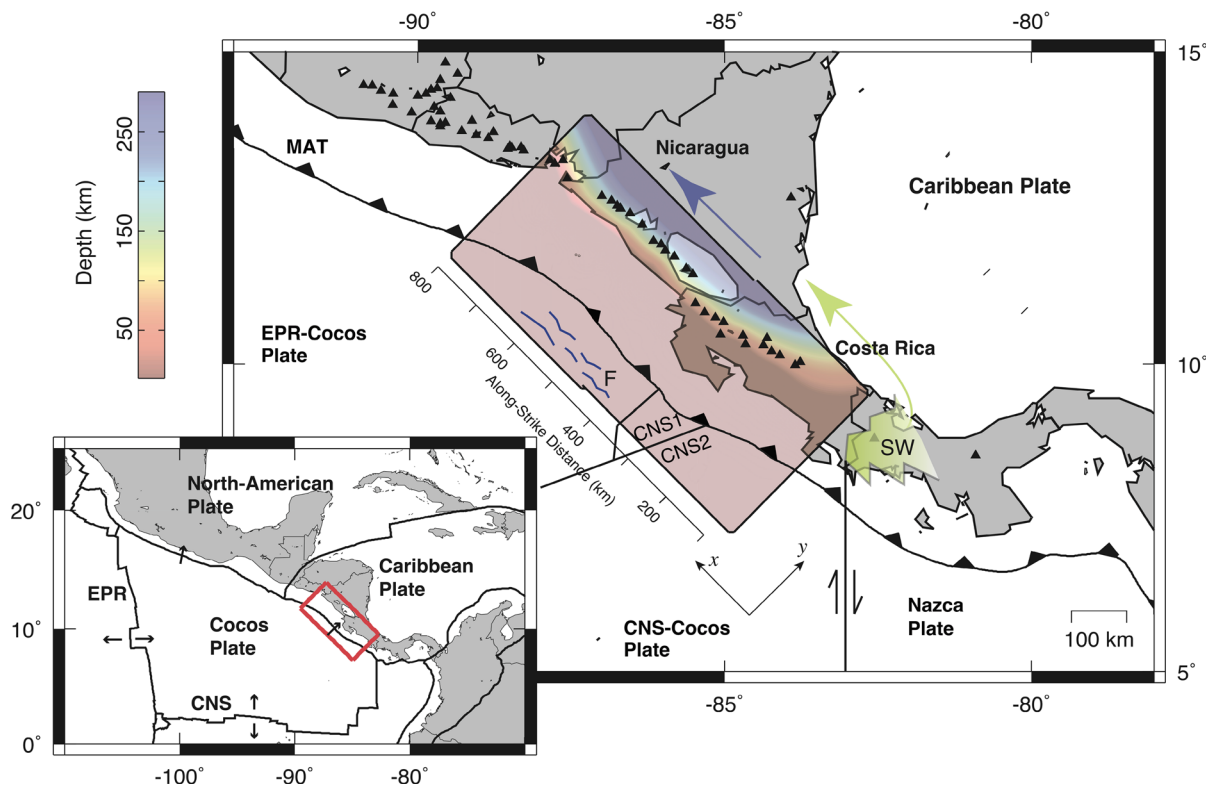


Figure 1

Map of the study area at the Costa Rica-Nicaragua subduction zone. Colors indicate the depth to the top of the subducted Cocos plate, as obtained from KYRIAKOPOULOS *et al.* (2015). Scale denotes along-strike distance (x-axis). 3D model extends from $x = 200$ km to $x = 700$ km, and from the trench landward until the slab reaches a depth of 300 km along the y-axis. Dashed black lines are the location of profiles A through D. Volcanoes are shown with black triangles. The Middle America Trench (MAT) runs approximately parallel to volcanic arc. Location of the Nicoya peninsula is shown. Plate boundaries between lithosphere generated at the East Pacific Rise (EPR) and lithosphere generated at the Cocos-Nazca Spreading Centre (CNS) are also shown (BARCHHAUSEN *et al.* 2001). Location of slab window (SW) is shown in light green (JOHNSTON and THORKELSON 1997), with light green arrow showing possible direction for oceanic-island basalt (OIB). B/La and Ba/La signal (blue arrow) increase in the northwest direction, indicating greater hydration in the mantle below Nicaragua. Inset shows study area (enclosed by red box) on a large-scale tectonic map. Black arrows denote plate motion. Plate boundaries are from BIRD (2003)

2010a, b), and different levels of hydration for the descending slab and overlying mantle (ABERS *et al.* 2003; SYRACUSE *et al.* 2008; RYCHERT *et al.* 2008; VAN AVENDONK *et al.* 2011; DINC *et al.* 2011). The geochemistry of arc magmas also varies along strike, with geochemical gradients in radiogenic isotope ratios, such as B/La and Ba/La, that are associated with fluid loss from the slab (PATINO *et al.* 2000; CARR *et al.* 2004). In addition, $^{208}\text{Pb}/^{204}\text{Pb}$ and $^{143}\text{Nd}/^{144}\text{Nd}$ ratios suggest that the magma source includes a component related to ocean-island basalt (OIB) from the Galapagos Hot Spot track (HERRSTROM *et al.* 1995; JOHNSTON and THORKELSON 1997; ABRATIS and WORNER 2001; HOERNLE *et al.* 2008). These data, together

with seismic anisotropy observations, have been used to argue for an along-strike flow of 6.3–19 cm/year within the mantle above the subducting Cocos plate in Costa Rica and Nicaragua (HOERNLE *et al.* 2008); flow is inferred to go from southeast to northwest (Fig. 1).

Many subduction zone processes, including the earthquake distribution, slab dehydration and arc volcanism, depend strongly on the thermal structure. A common approach to study the temperature distribution is to create two-dimensional (2D) steady-state numerical models of the subduction system (oceanic plate, overriding plate, and viscous mantle wedge) in which dynamically calculated mantle

wedge flow is driven by a kinematically prescribed subducting plate (e.g., PEACOCK 1996). Three key factors control the thermal structure of a subduction zone: the temperature of the incoming oceanic plate (slab), the plate convergence rate, and the flow pattern of the overlying mantle wedge. The temperature of the slab is primarily a function of its age, with heat being transferred by conduction. In the mantle wedge, however, heat is transferred mainly by the motion of the viscous mantle. In the context of fluid dynamics, the downward motion of the descending oceanic plate drags the overlying mantle by viscous coupling and sets up a forced-convection flow pattern, i.e., corner flow (BATCHELOR 2000).

Several 2D thermal models have been developed for the Costa Rica-Nicaragua subduction zone. The objective of these models varies, and they can be roughly classified into two categories:

1. Models to study the relationship between hydrothermal circulation and shallow slab temperatures.
2. Models to study the role of viscous wedge flow in deep metamorphic and dehydration reactions within the slab.

The first category is reasonably well studied. These studies show that significant hydrothermal circulation must occur in the shallow (<1 km) oceanic crust, to explain the observed surface heat flow along the MAT in Central America (FISHER *et al.* 2003; HUTNAK *et al.* 2008; HARRIS *et al.* 2010a). Hydrothermal circulation cools the oceanic crust and provides a relatively good match between crustal temperatures and distribution of seismicity (HARRIS and WANG 2002; KUMMER and SPINELLI 2008; HARRIS *et al.* 2010b; COZZENS and SPINELLI 2012; ROTMAN and SPINELLI 2013). For the second category, PEACOCK *et al.* (2005) demonstrated that a non-Newtonian mantle rheology is needed to sustain the high temperatures required for mantle melting and arc volcanism. This also results in an oceanic crust that is fully dehydrated and transformed to eclogite at depths of 70–100 km. However, they do not find significant variations in the thermal or flow structure along the strike of the subduction zone, which would be needed to fit the along-margin variations in arc geochemistry.

There are multiple factors that may explain the discrepancy between 2D models and the observed geochemistry. These include possible along-strike changes in the thermal state of the incoming oceanic plate (ROSAS *et al.* 2015, submitted) or changes in the amount of water released into the mantle (ABERS *et al.* 2003; SYRACUSE *et al.* 2008; RYCHERT *et al.* 2008; Van AVENDONK *et al.* 2011; DINC *et al.* 2011). An important one, however, is the intrinsic two-dimensionality of the corner flow model. It is known that geometrical factors such as along-strike variations in slab dip or trench curvature can induce along-strike mantle flow (KNELLER and van KEKEN 2008; BENGTON and van KEKEN 2012; WADA *et al.* 2015). Such characteristics are present in Central America (Fig. 1). In this region, the Cocos plate changes its dip from approximately 70° in Nicaragua to 45° in Central Costa Rica at depths greater than 70 km. The change occurs over an along-strike distance of 200 km.

In this study, we present the first three-dimensional (3D) model of the thermal structure of the Costa Rica-Nicaragua subduction zone. Our approach is similar to previous 2D models, as we incorporate a subducting slab that drives mantle wedge flow by viscous coupling. However, we consider a three-dimensional slab with a non-Newtonian rheology for the mantle wedge, using the most up-to-date geometry for the Cocos plate. This is expected to induce significant lateral flow in the mantle wedge, therefore changing the overall temperature distribution relative to 2D models. Our objectives are to quantify these differences and provide a more detailed description of the thermal structure of this subduction zone.

2. Model Set Up

The numerical models use a kinematic-dynamic approach to model the steady-state thermal structure of the subduction zone (van KEKEN *et al.* 2008, 2002; CURRIE *et al.* 2004). The subducting oceanic plate and overriding continental plate have a fixed geometry and convergence rate. The mantle wedge has a viscous rheology and flows in response to the imposed subduction dynamics. The advantage of this approach over a completely dynamic subduction zone is that it allows for a much higher resolution of the thermal

structure, especially in the mantle wedge corner region (BILLEN 2008). The disadvantage is that we neglect any dynamic factors, such as slab rollback or roll forward, which might induce 3D mantle flow as well.

To investigate 3D mantle wedge flow and the resulting temperature distribution of the Costa Rica–Nicaragua subduction zone, we use a three-dimensional finite-element mesh of the Costa Rica–Nicaragua subduction zone. The mantle wedge flow and thermal structure are computed using the equations of mass, momentum and energy. In that order, the equations are:

$$\nabla \cdot \mathbf{v} = 0, \quad (1)$$

$$\nabla P - \nabla \cdot \sigma = 0, \quad (2)$$

$$\nabla \cdot (k \nabla T) - \rho c_p (\mathbf{v} \cdot \nabla T) + A = 0, \quad (3)$$

where \mathbf{v} is the velocity, P is the dynamic pressure, σ is the deviatoric stress tensor, T is the temperature, k is the thermal conductivity, A is the rate of radiogenic heat production, ρ is the density, and c_p is the specific heat. In the calculations, the mantle is assumed to be a Boussinesq fluid with infinite Prandtl number, and flow in the mantle wedge is driven only by the subducting plate. The models use the finite-element code PGCtherm3D. This code is the three-dimensional version of PGCtherm2D, which has been previously benchmarked (van KEKEN *et al.* 2008) and used in other studies of different subduction zones (e.g., CURRIE *et al.* 2004; WADA *et al.* 2008; WADA and WANG 2009; WANG *et al.* 2015). PGCtherm3D was also used in a recent 3D modeling study of the northeast Japan subduction zone (WADA *et al.* 2015).

The three main units in the model are the overriding Caribbean plate, the subducting Cocos plate and the viscous mantle wedge; smaller units such as the sediment layer of the oceanic plate or the upper and lower continental crust are considered as part of these main units. The rigid overriding plate consists of a 35 km-thick crust and the top 5 km of upper mantle. This crustal thickness is consistent with the average Moho depth for Central America (MACKENZIE *et al.* 2008; MANEA *et al.* 2013). The geometry of the subducting plate is from KYRIAKOPOULOS *et al.* (2015). The subducting plate has a total thickness of

100 km, and it is assumed that this includes the oceanic sediments, crust and mantle lithosphere, as well as sub-lithospheric mantle that is entrained with the subducting lithosphere. The model domain extends from south Costa Rica to Nicaragua. We selected this region due to the strong along-margin variations in slab dip at depths ~70 km, which changes from approximately 70° in Nicaragua to 45° in central Costa Rica. Further south, the Cocos plate is difficult to observe because of the lack of Wadati–Benioff seismicity and arc volcanism (PROTTI *et al.* 1995). The area may correspond to a slab window formed by subduction of the Cocos–Nazca spreading centre from late Miocene to late Pliocene (JOHNSTON and THORKELSON 1997; ABRATIS and WORNER 2001), as shown in Fig. 1. The x -axis in our models is approximately aligned with the trench, the y -axis is in the landward direction, and the z -axis is the depth. The origin of the model grid is at -84°W , 7°N , and therefore, the model domain extends from $x = 200$ to $x = 700$ km. The trench corresponds to the seaward boundary of the model. The location of the backarc (landward) boundary is taken to be where the top of the oceanic plate is at a depth of 300 km; this keeps our modeling domain in the upper mantle. As the slab dip varies along the strike of the subduction zone, the distance between the trench and backarc boundary is variable, ranging between 200 and 300 km from the wedge corner. Tests show that the location of the backarc boundary has only a minor effect on temperatures in the mantle wedge, as long as the distance from the wedge corner to the boundary does not change by more than 200 km along the strike.

The thermal parameters for each model material follow those used by HARRIS *et al.* (2010b) and are given in Table 1. The overriding plate has a velocity of 0 cm/year, and the subducting plate has an assigned convergence velocity of 9.1 cm/year, in agreement with the average velocity in our modeling area (DEMETS 2001). For the mantle wedge, we present models with either an isoviscous rheology (viscosity of 10^{21} Pa s) or a power-law (non-Newtonian) rheology. The latter is based on the flow law for dislocation creep of wet olivine (KARATO and WU 1993):

$$\eta = A(\dot{\epsilon})^{\left(\frac{1}{n}-1\right)} \exp\left(\frac{E}{nRT}\right) \quad (4)$$

Table 1

Radioactive heat generation (A), thermal conductivity (k), density (ρ) and heat capacity (c_p) for the subdomains in the numerical models

Subdomain	A ($\mu\text{W}/\text{m}^3$)	k ($\text{W}/(\text{m}\text{K})$)	ρ (g/cm^3)	c_p ($\text{J}/(\text{kg K})$)
Continental crust	0.2	2.9	3.3	1250
Mantle wedge	0.02	3.1	3.3	1250
Oceanic slab	0.2	2.9	3.3	1250

The thermal diffusivity (K) is given by $k/\rho c_p$

where $A = 28,968.6 \text{ Pa s}^{1/n}$ is the pre-exponential factor, $\dot{\epsilon}$ is the strain rate, $E = 430 \text{ kJ/mol}$ is the activation energy, R is the universal gas constant, T is the temperature, and $n = 3$ is the power-law exponent.

The boundary conditions for the model are shown in Fig. 2. The top of the model is rigid with a temperature of 0°C , and the bottom of the model corresponds to the base of the oceanic plate, which has a velocity of 9.1 cm/year and temperature of 1450°C . Free-slip and insulating boundary conditions are used on the side boundaries at $x = 200 \text{ km}$ and $x = 700 \text{ km}$, such that $v_x = 0$ and there is no

heat flow through these boundaries. The effect of the boundary conditions on the modeling results is discussed in Appendix. At the oceanic boundary, a fixed velocity of 9.1 cm/year is assigned. The temperatures along this boundary are based on the GDH1 oceanic plate cooling model (STEIN and STEIN 1992), using the age of the plate at each point along the trench. The complete oceanic boundary temperature can be seen in Fig. 2a. Three age domains are included. Lithosphere generated at the Cocos-Nazca Spreading Centre (CNS) is divided into two sections: CNS1 and CNS2 (von HUENE *et al.* 2000; BARCKHAUSEN *et al.* 2001). These segments have ages of 17.5–20, and

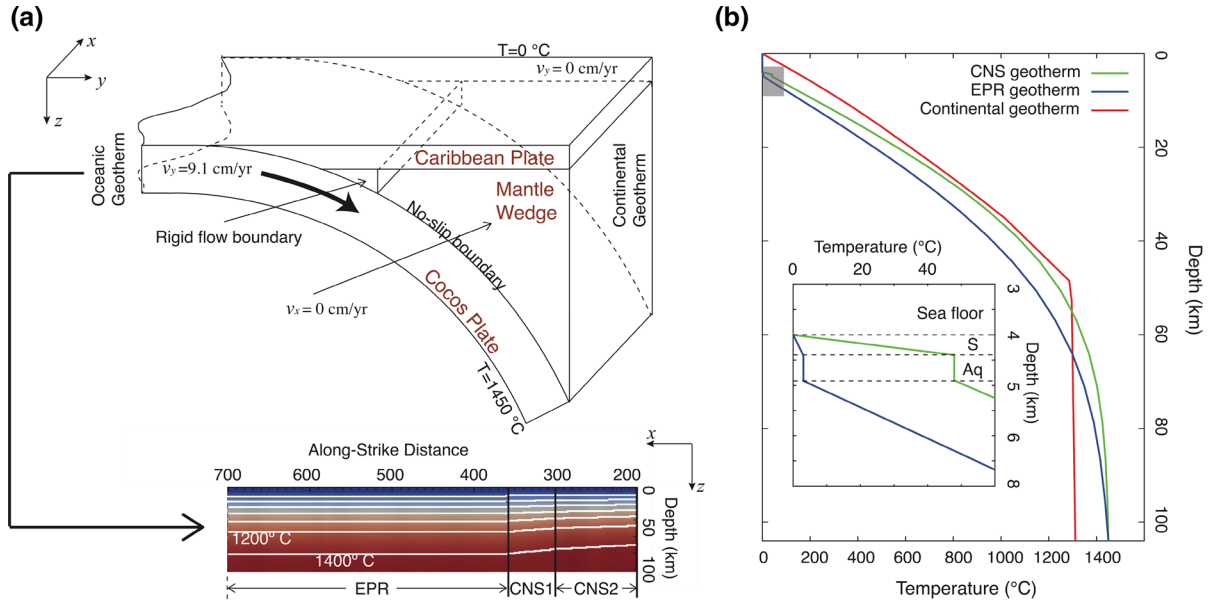


Figure 2

a Schematic diagram of the 3D model and boundary conditions. The 2D temperature boundary condition for the oceanic boundary is shown, with isotherms shown every 200°C . Location of the boundary between CNS and EPR lithosphere is shown. b Typical geotherms for CNS (green) and EPR (blue) oceanic lithosphere. Inset shows the oceanic geotherms at shallow depths, with sediments (S) and aquifer (Aq) having thicknesses of 400 m and 500 m, respectively

20–24 Myear, respectively. An age of 24 Myear is used for lithosphere generated at the East Pacific Rise (EPR). The boundary between EPR and CNS2 lithosphere is found offshore the Nicoya peninsula (Fig. 1); in our coordinate system is located at approximately $x = 360$ km. At each point along the trench, the 1D oceanic geotherm incorporates the effects of sedimentation and sediment permeability, following LANGSETH and SILVER (1996), HARRIS and WANG (2002) and HARRIS *et al.* (2010b). In this area, temperatures at the uppermost oceanic crust (aquifer) may be affected by hydrothermal circulation. HARRIS *et al.* (2010b) showed that the offshore heat flow data are consistent with ventilated hydrothermal circulation for the EPR segment and insulated hydrothermal circulation for the CNS segment. In their models, hydrothermal circulation is allowed to continue to greater depths after subduction by introducing conductivity proxies in the crustal aquifer (DAVIS *et al.* 1997). Our geotherms use the thermal structure proposed by HARRIS *et al.* (2010b) for the oceanic boundary but do not include conductivity proxies for the aquifer. Our approach is thus similar to that employed by LANGSETH and SILVER (1996) and HARRIS and WANG (2002). Figure 2b shows typical geotherms for EPR and CNS sections.

At the backarc boundary, stress-free conditions are used. No heat flow is assumed through this boundary, and the inflow–outflow transition is determined dynamically. The backarc geotherm is given by a steady-state equilibrium geotherm for a continental plate with a surface heat flux of 90 mW/m^2 , in agreement with observed backarc temperatures (CURRIE and HYNDMAN 2006). This geotherm intersects a mantle adiabatic gradient with a potential temperature of 1295°C at an approximate depth of 50 km (Fig. 2b). The geotherm temperatures are assigned to the rigid overriding plate and the region of the mantle wedge with flow into the model domain.

Flow within the mantle wedge is driven by the subducting oceanic plate. Therefore, we employ a no-slip boundary condition between the downgoing plate and the lower boundary of the mantle wedge. The upper wedge boundary has a fixed velocity of 0 cm/year . For computational efficiency, a rigid vertical flow boundary is placed in the wedge. This is also

consistent with serpentinization of the forearc mantle, which is proposed to decouple the subducting slab from the mantle (MANEA *et al.* 2005, 2008; WADA *et al.* 2008). The boundary is located at the point at which the slab reaches a depth of 70 km, and it extends from the surface of the slab to the base of the upper plate. This location is consistent with observations that show that stagnation of the wedge corner is required to fit observations of a rapid landward increase in surface heat flow, from low values in the forearc to high values near the volcanic arc and into the backarc (WADA *et al.* 2008; WADA and WANG 2009). In the models, there are high gradients in pressure and temperature near the mantle wedge corner and along the surface of the slab, especially when a non-linear rheology is used (Eq. 4). Thus, our models use a variable element size in the direction of subduction, where elements are as small as a few meters in the mantle wedge tip and as large as $\sim 10 \text{ km}$ in the upper crust and deep slab. Along the strike of the subduction zone, the element width is 2 km. These sizes are based on benchmark tests (van KEKEN *et al.* 2008; BENGTSON and van KEKEN 2012). In total, we employ 1,138,800 cubic elements that give a total of 9,262,617 grid nodes.

To assess the effect of 3D processes on the thermal structure, we also present 2D models at several locations along the subduction zone (Fig. 1). These 2D models are later compared to cross-sections extracted from the 3D model at the location of each profile. From south to north, the profiles are: profile A and B, located in south and central Costa Rica, respectively; profile C, located near the Costa Rica-Nicaragua border; and profile D, located in central Nicaragua. Profile A is located in a region in which there is a change of almost 25° in the dip of the slab over an along-strike distance of 200 km. For the other profiles, there are no significant along-margin changes in the geometry of the plate. These 2D models also use PGCtherm3D, but are only 100 m wide, with no variations in slab geometry (i.e., they have a 2D structure). The models have the same material properties and boundary conditions as those in the full 3D model. Given that convergence of the Cocos plate in the MAT along Costa Rica-Nicaragua is mostly trench-perpendicular ($\sim 10^\circ$ obliquity) (DEMETS 2001) and that the trench is almost straight in our

study region, our 2D profiles are taken parallel to the convergence direction.

3. Results

Flow in the mantle wedge is a primary control factor on the thermal distribution of a subduction zone, especially beneath the volcanic arc. The nature of flow depends on the rheology of the mantle wedge (e.g., van KEKEN *et al.* 2002). Shear-wave splitting studies demonstrate that the dislocation creep is the dominant deformation mechanism in the mantle wedge (KNELLER and van KEKEN 2008; LONG and SILVER 2008; HOERNLE *et al.* 2008; SOTO *et al.* 2009). However, we also present isoviscous models to gain a basic understanding of the factors that control the direction and magnitude of mantle wedge flow.

It is illustrative to start with a brief discussion of 2D models. Figure 3a shows the basic structure of a 2D corner flow for an isoviscous mantle wedge for profile A. In a subduction zone, the downward motion

of the slab drags the overlying mantle through viscous coupling (yellow ellipse). This creates a region of low pressure near the wedge corner (green circle) which induces flow that brings hot mantle from the backarc to replenish the lost material. The magnitude and size of this low-pressure area depends on the dip of the slab, with shallower dips tending to create lower pressures and a larger low-pressure region (TURCOTTE and SCHUBERT 2002; MANEA and GURNIS 2007). As a result of this flow pattern, the thermal structure of the subduction zone has two distinct regimes. The forearc is relatively cool, owing to conductive cooling by the underlying oceanic plate; the arc and backarc regions are heated by the mantle wedge flow.

For an isoviscous rheology, the constant viscosity of the mantle allows flow through the backarc boundary at any depth. However, a dislocation creep rheology is temperature dependent (Eq. 4) and thus flow is generally limited to temperatures greater than 1200 °C (van KEKEN *et al.* 2002; CURRIE *et al.* 2004). Figure 3b shows a 2D model that uses a dislocation

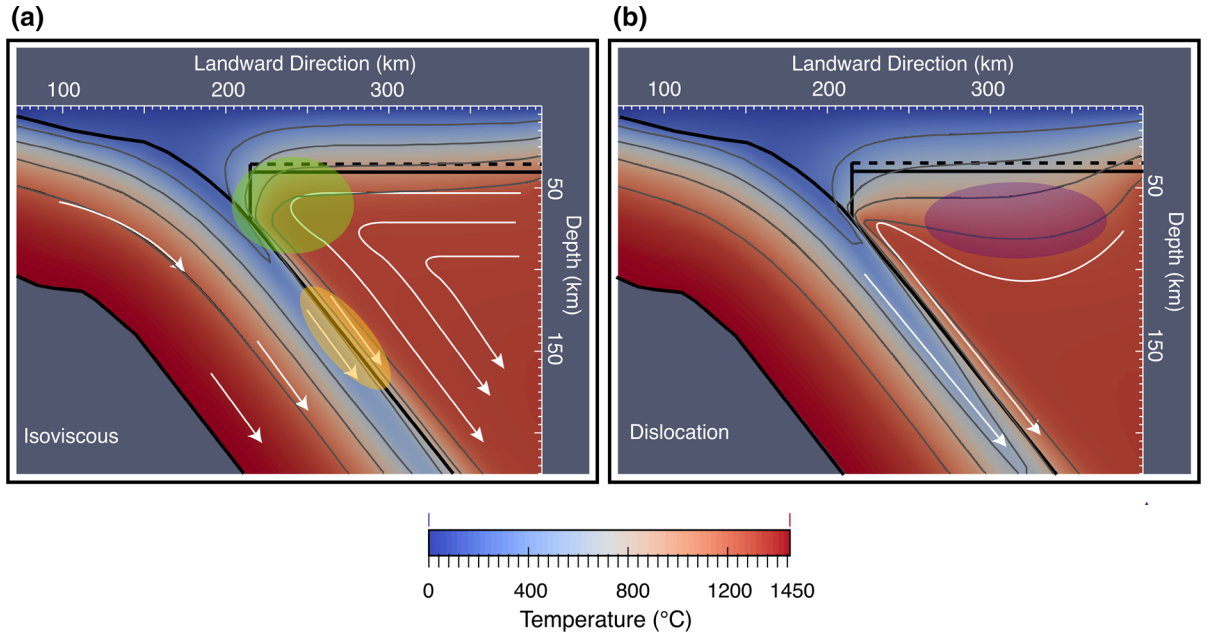


Figure 3

Two-dimensional (2D) corner flow models for **a** an isoviscous and **b** a dislocation creep wedge. Figures are for profile A. Black dashed line indicates the continental Moho. White arrows are streamlines. Green circle shows the low-pressure corner, which induces flow that brings hot mantle from the backarc. Yellow ellipse shows viscous coupling between slab and mantle wedge. Purple ellipse shows the stagnant lid for a dislocation creep rheology. Temperature contours are shown every 300 °C

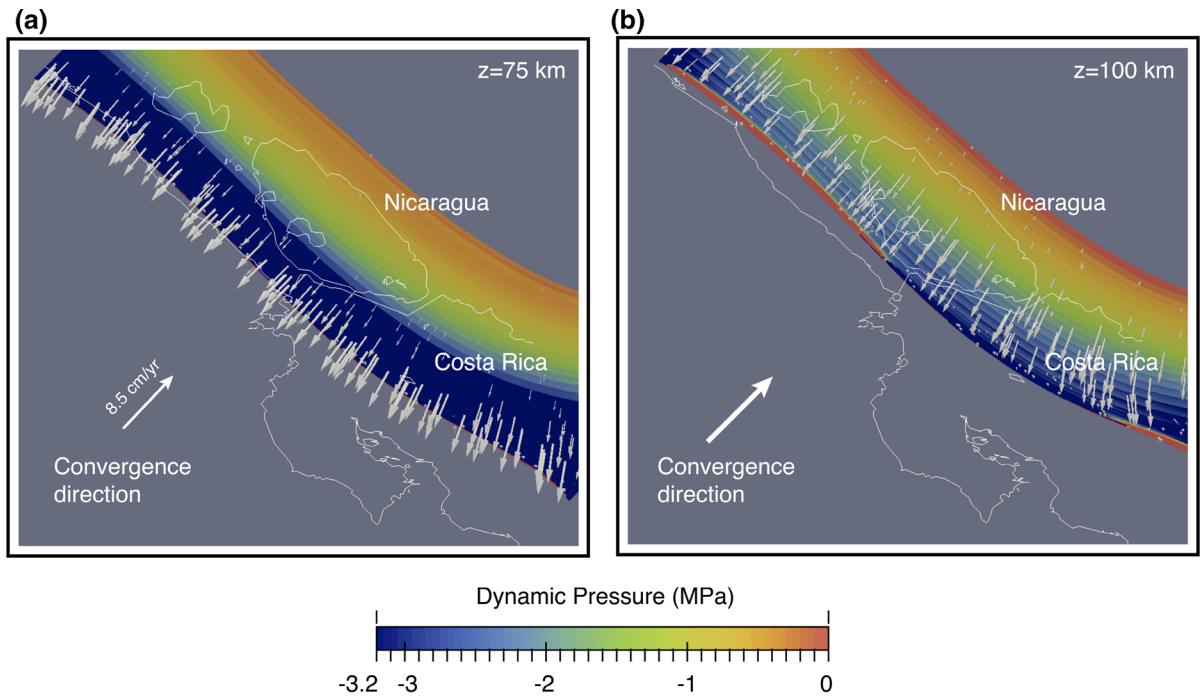


Figure 4

Dynamic pressure for the 3D model in horizontal planes located at depths of **a** 75 km and **b** 100 km. Color scale the magnitude in MPa. Gray arrows mantle wedge flow along each plane. Mantle wedge flow is mostly parallel (2D) to convergence direction below Nicaragua and northern Costa Rica. From mid-Nicoya to southern Costa Rica, mantle flow has an along-strike component (3D). Mantle flow departs from the 2D corner flow in response to changes in the low-pressure region (blue), which in turn are associated with changes in the dip of the slab

creep mantle wedge rheology. With this rheology, flow enters the model domain at a greater depth along the backarc boundary, and it is more strongly focused upward into the wedge corner, compared to the isoviscous model. As a result, the temperature in the mantle wedge corner is ~ 100 to 200 °C higher than for the isoviscous case. However, the upper part of the mantle wedge is essentially stagnant, leading to cool temperatures in this area (~ 800 °C). This region is known as the stagnant lid and is shown in Fig. 3b by a purple ellipse.

3.1. Three-Dimensional Flow Field

In a three-dimensional subduction zone, the subducting plate also drags the overlying mantle downward, inducing corner flow. However, features such as along-strike changes in slab dip, obliquity, or trench curvature will induce lateral pressure gradients, which can lead to along-strike flow (KNELLER and van KEKEN 2008; BENGTSON and van KEKEN

2012). For the case of Costa Rica-Nicaragua, along-strike variations in the dip of the Cocos plate (Fig. 1) induce changes in the dynamic pressure within the mantle wedge (Fig. 4). In response to this change, a component of along-strike flow is produced in the mantle wedge, with flow directed toward the southeast, from the region of high slab dip (70°) below Nicaragua to low slab dip (45°) below Costa Rica. This is consistent with the idea that a shallower dip induces lower pressures in the mantle wedge (e.g., TURCOTTE and SCHUBERT 2002; MANEA and GURNIS 2007), and thus the corner flow is deflected towards the area of lower slab dip. The total flow field of the mantle wedge is therefore a combination of a 2D corner flow and lateral flow.

Figure 5 shows the modeled wedge flow field for the isoviscous and dislocation creep cases. The flow field is visualized through streamlines that track the path of particles. The color scale denotes along-strike velocity (v_x), with positive values indicating north-westward flow. The dominant component of the flow

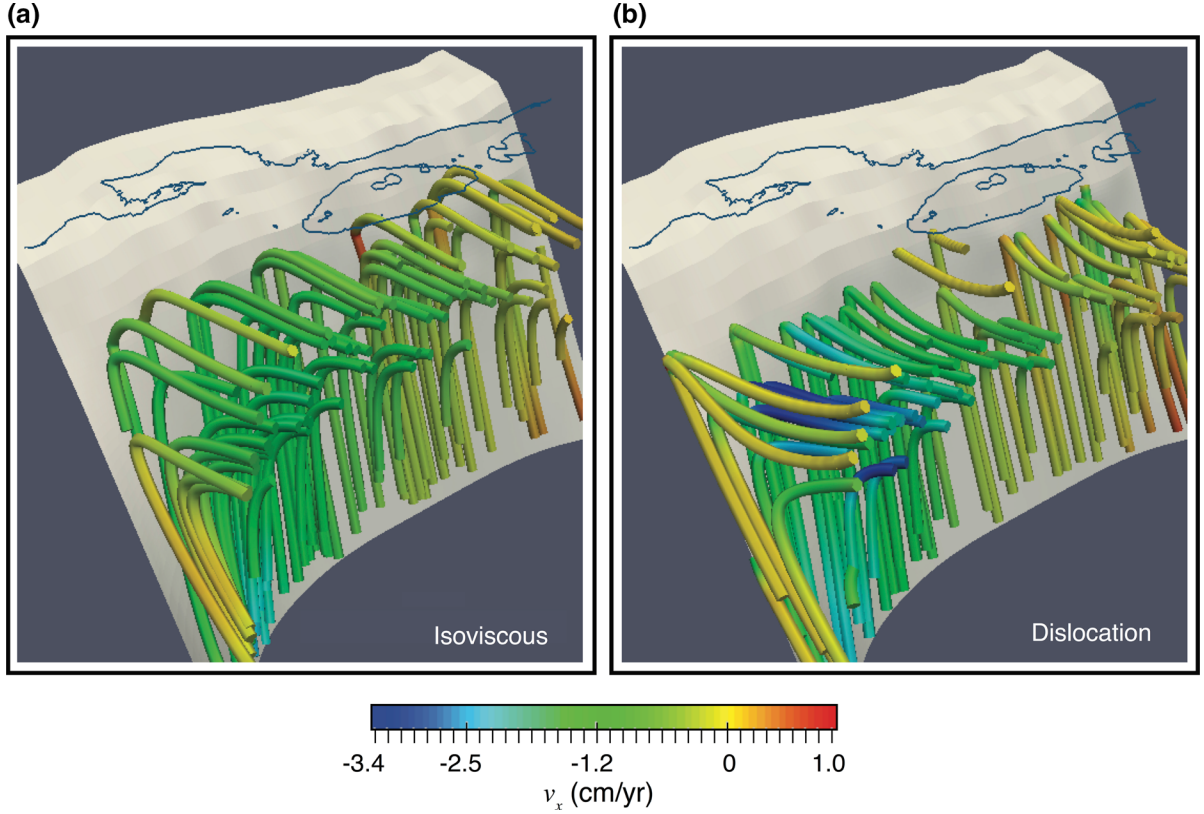


Figure 5

Three-dimensional flow field in the mantle wedge for **a** an isoviscous and **b** a dislocation creep rheology. Color scale denotes along-strike velocity, v_x , with blue denoting southeast flow and red denoting northwest flow. Maximum v_x for the isoviscous and dislocation creep models (not shown in figure) is -2.5 and -4.0 cm/year, respectively

field is the slab-driven corner flow, where particles are pulled toward the wedge corner and then descend with the subducting plate. As seen in the 2D models, a dislocation creep rheology leads to a strong focusing of flow toward the wedge corner (Fig. 3b), whereas an isoviscous wedge has subhorizontal flow in the upper part of the wedge (Fig. 3a). In both cases, the flow also exhibits an along-strike component. This is largest below Costa Rica in the southern part of the model domain, where there are along-strike changes in slab dip. In the isoviscous case (Fig. 5a), a maximum along-strike velocity of -2.5 cm/year is observed, whereas the dislocation creep rheology results in a maximum along-strike velocity of over -4 cm/year. This difference is caused by a lower mantle viscosity due to the higher temperatures in the dislocation creep model; flow is

concentrated in the central wedge region where temperatures are highest. The along-strike flow is minimal in the northern part of the model area, as there are only minor dip variations here.

It is important to mention that our current choice of boundary conditions could have an effect on the observed mantle flow. The $v_x = 0$ restriction imposed on the side boundaries affects the flow pattern, and as a result, our 3D model may underestimate the along-strike flow component. A detailed discussion of the effect of the boundary conditions in mantle flow is given in Appendix.

3.2. Three-Dimensional Thermal Structure

Our three-dimensional thermal model for Costa Rica-Nicaragua is shown in Fig. 6a for a dislocation

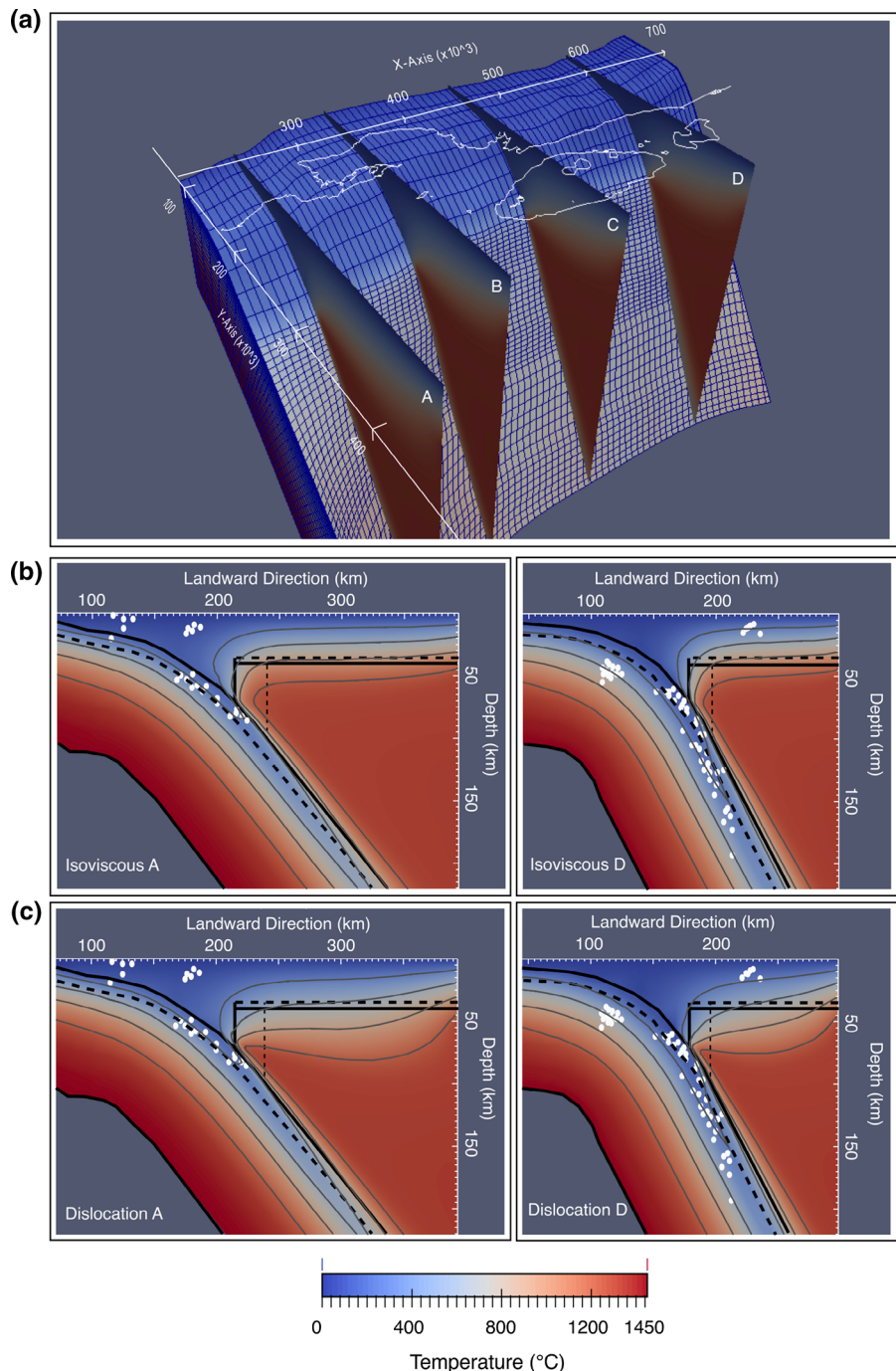


Figure 6

a Three-dimensional (3D) thermal model of the Costa Rica-Nicaragua subduction zone, with location of profiles A through D shown. The rheology for this model is dislocation creep. Cross-sections extracted from 3D model for profiles A and D are shown in two-dimensional view for **b** an isoviscous and **c** a dislocation creep rheology. Temperature contours are shown for every 300 °C. White dots are seismicity from the TUCAN (ABERS *et al.* 2004) and CRSEIZE (http://es.ucsc.edu/~hdeshon/crseize_homepage.html) deployments. Thick dashed lines represent the oceanic and continental Moho. Thin dashed line represents location of volcanic arc geotherm (Fig. 10a)

creep rheology. The location of profiles A through D is shown. The detailed model results are also shown for profiles A and D for an isoviscous (Fig. 6b) and dislocation creep rheology (Fig. 6c). The large-scale temperature field for profile A is similar to that seen in the 2D models (Fig. 3). If the wedge has an isoviscous rheology, isotherms are subhorizontal in the shallow backarc (Fig. 6b). In contrast, a dislocation creep rheology leads to a strong focusing of flow from depth into the wedge corner and a cool stagnant lid is created in the backarc (Fig. 6c).

To assess the effects of along-margin mantle flow, Figs. 7 and 8 show the difference between 3D and 2D mantle wedge temperatures and the along-strike mantle flow for an isoviscous and non-Newtonian rheology, respectively. For both cases, the largest temperature difference is observed in profile A. For profiles B, C and D, the magnitude of the difference decreases in the northwestward direction. This result is consistent with the location of strong along-margin slab curvature, mostly located in the southeast side of our domain area (Fig. 1), which creates pressure gradients that drive the flow in the southeastward direction (Fig. 4).

For an isoviscous rheology, the along-strike flow decreases temperatures in the 3D model by 10–30 °C with respect to the 2D model along profile A (Fig. 7). The along-strike component of the flow has a magnitude of ~ 1.5 cm/year. For profile B, temperatures do not change appreciably in the mantle wedge, despite the stronger along-strike flow (~ 2 cm/year). The difference between profiles A and B can be understood by considering the motion of a single fluid element in the mantle. Given the higher along-strike velocities along profile B, a fluid element in this area would have less time to cool than a fluid element in the vicinity of profile A at a given distance from the backarc boundary. The result is that 3D flow cools down the mantle more efficiently for profile A than for profile B. For profiles C and D, there are no variations in mantle wedge temperatures between 2D and 3D models and almost no along-strike flow (<1 cm/year), indicating the mantle flow in this region is mostly 2D corner flow.

For a mantle with a dislocation creep rheology (Fig. 8), the temperature differences between 2D and

3D models are largest for profile A, but the effect of 3D flow is opposite to that in the isoviscous case. For this profile, the mantle wedge in the 3D model is up to 50 °C hotter than the 2D model, with the largest change in the uppermost mantle (stagnant lid). The along-strike flow has a maximum magnitude of ~ 4 cm/year for profile A. The thermal changes decrease in the northwest direction. Profile B still shows a difference of 20 °C, with an along-strike flow of ~ 2.5 cm/year. For profiles C and D, only minor changes in the mantle wedge temperatures are observed. In these models, the viscosity of the mantle wedge depends on both the temperature and stress (Eq. 4), which results in a more complex feedback between the flow field and thermal structure than for the isoviscous case. In general, however, the along-strike flow for the dislocation creep case has a relatively higher magnitude than in the isoviscous case. This rapid flow may limit the thickness of the stagnant lid, and as a result, the upper part of the mantle wedge will be somewhat warmer compared to a purely 2D model.

On all profiles, moderate changes in thermal structure are observed in a local region (<5 km wide) in the wedge corner near the stagnant wedge boundary (Figs. 8, 9). This region is characterized by strong pressure and thermal gradients that require high resolution to properly resolve for the temperature (van KEKEN *et al.* 2002). Thus, the temperatures in the wedge corner have some uncertainty that may arise from numerical artifacts.

4. Thermal Structure of the Costa Rica-Nicaragua Subduction Zone

The thermal structure of a subduction zone is a crucial control on key processes, including magmatism, slab metamorphism and dehydration, and earthquake distribution. Here, we examine the temperatures of the subducting slab and mantle wedge of our full 3D model with a dislocation creep rheology (Fig. 6a). Seismic anisotropy studies for Central America suggest flow by dislocation creep is the most appropriate rheology (HOERNLE *et al.* 2008).

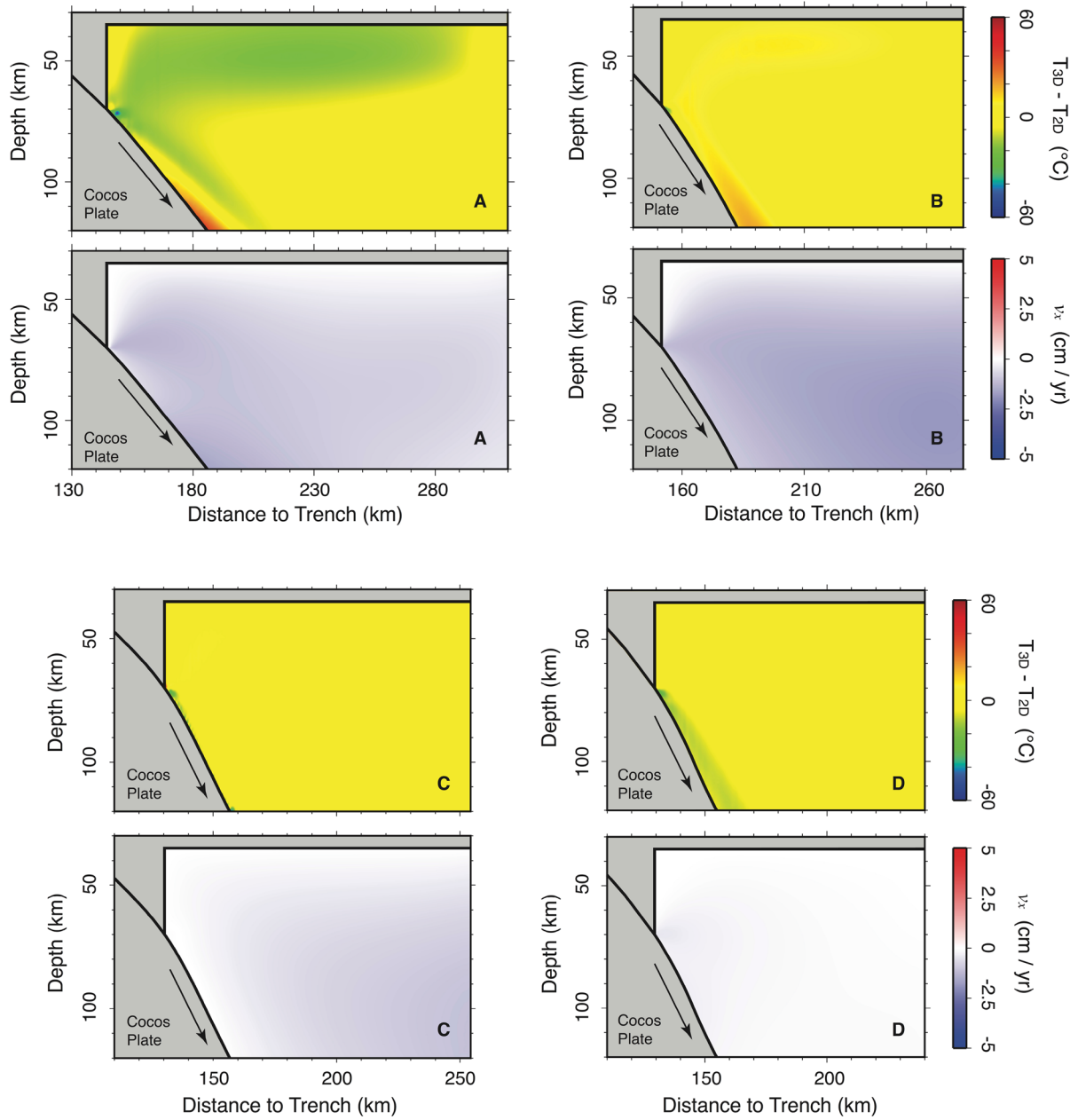


Figure 7

Temperature difference ($T_{3D} - T_{2D}$; *upper plot*) and along-strike velocity component (v_x ; *lower plot*) for profiles A through D with an isoviscous (10^{21} Pa s) mantle wedge. Black arrow denotes subduction direction. Negative sign in the along-strike velocity indicates southeastward flow

4.1. Megathrust Earthquake Seismogenic Zone

We first address the implications of the 3D thermal model for megathrust earthquakes, which are earthquakes that occur on the subduction interface. The seismogenic zone corresponds to the part of

the interface that exhibits velocity-weakening behavior, and this may depend on interface temperatures (e.g., HYNDMAN *et al.* 1997). The updip limit is usually placed at temperatures of 100–150 °C, while the downdip limit is at either 350–450 °C or the

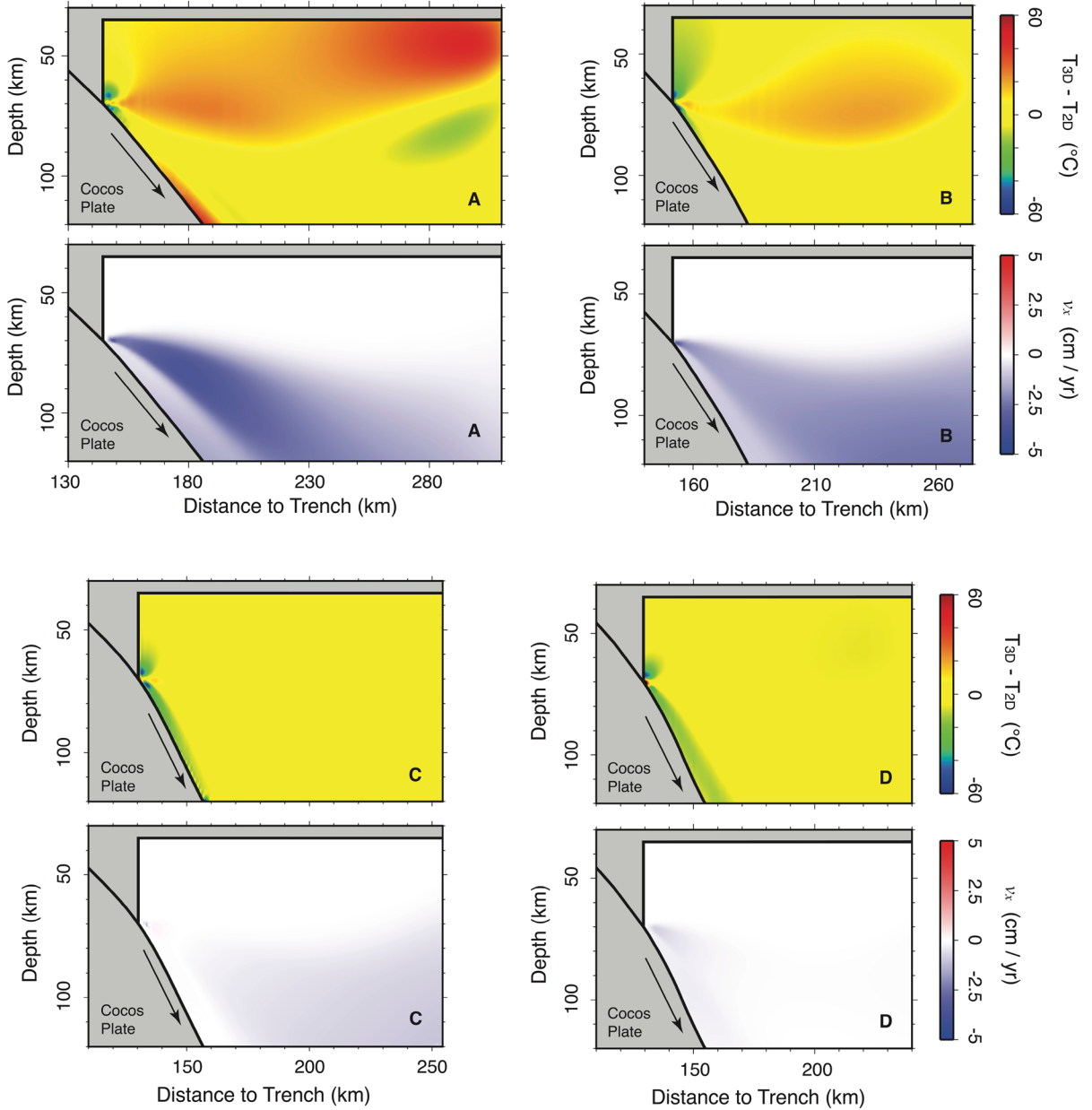


Figure 8

Same as in Fig. 8, but for a non-Newtonian mantle wedge that flows through dislocation creep (Eq. 4)

intersection between the interface and the upper plate Moho.

Figure 9 shows pressure–temperature (PT) paths for the surface of the Cocos plate for profiles A through D, for both the 3D (solid line) and 2D (dashed line) models with a dislocation creep mantle;

note that pressure has been converted to depth using the material density. A temperature of 100 °C occurs at a depth of 15–20 km for the southern profiles (A and B), and at ~10 km depth for the northern profiles (C and D). For all profiles, a temperature of 350 °C occurs at depths greater than 60 km. The

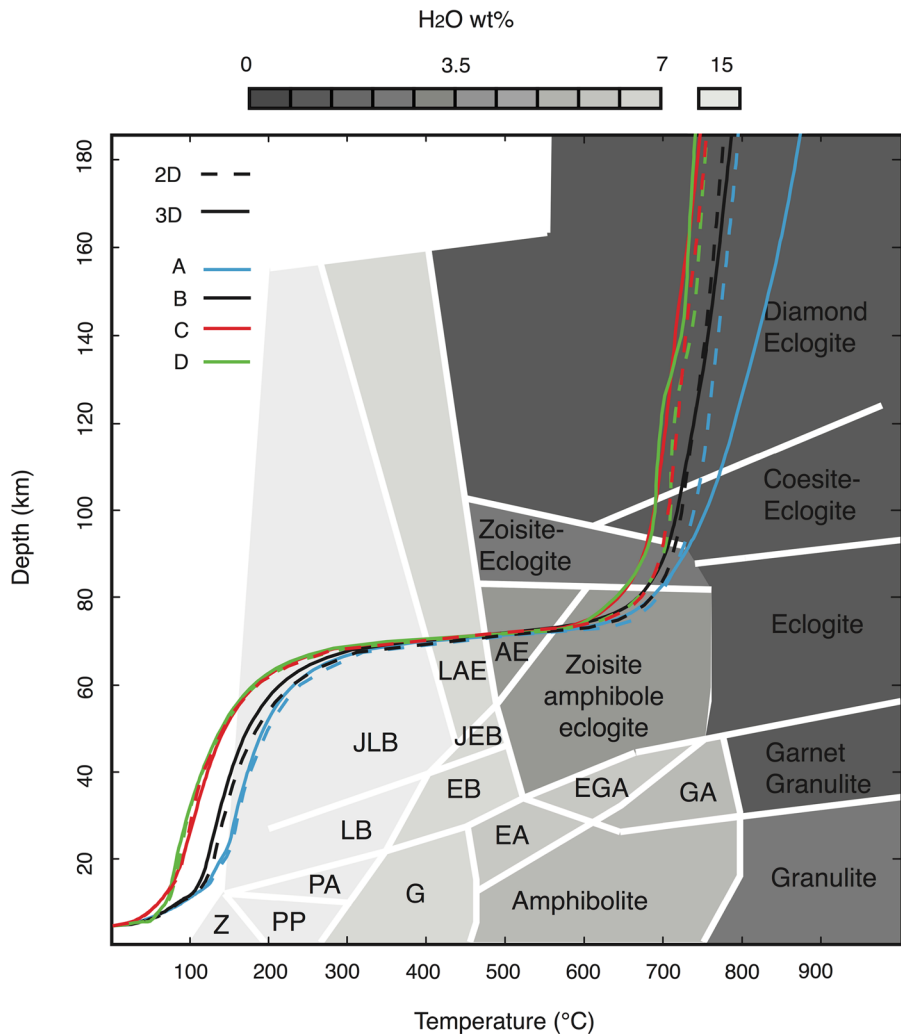


Figure 9

Phase diagram for mid-ocean ridge basalt (MORB), showing pressure–temperature (PT) paths for the surface of the slab for profiles A through D. *Solid lines* are for 3D models, and *dashed lines* are for 2D models. *Shades of gray* denote water content. Phase diagram from HACKER *et al.* (2003). Metamorphic facies: A amphibolite, AE amphibole eclogite, EA epidote amphibolite, EB epidote blueschist, EGA epidote garnet amphibolite, G greenschist, GA garnet amphibolite, JLB jadeite lawsonite blueschist, JEB jadeite epidote blueschist, LAE lawsonite amphibole, JLB jadeite lawsonite blueschist, LB lawsonite blueschist, PP prehnite pumpellyite, Z zeolite

Moho depth for the Caribbean plate is 35 km (MACKENZIE *et al.* 2008). Thus, it is likely that the downdip limit of the seismogenic zone corresponds to the Moho intersection and not the 350 °C isotherm. This is consistent with the conclusion of HARRIS *et al.* (2010b).

Figure 10 shows a map view of the location of the 100 °C isotherm on the subduction interface for our 3D model, as well as the location of the Moho intersection (corresponding to a slab depth of 35 km).

There is an abrupt seaward shift in the position of the 100 °C isotherm at the position of the Nicoya Peninsula. This point marks the change from oceanic lithosphere created at the East Pacific Rise (EPR) in the north and Cocos-Nazca Spreading Centre (CNS) in the south (Fig. 1). At the trench, the incoming EPR lithosphere is cooler than the CNS lithosphere (Fig. 2b), which translates to a cooler subduction interface and a more landward location of the 100 °C isotherm for the EPR segment. For the CNS segment,

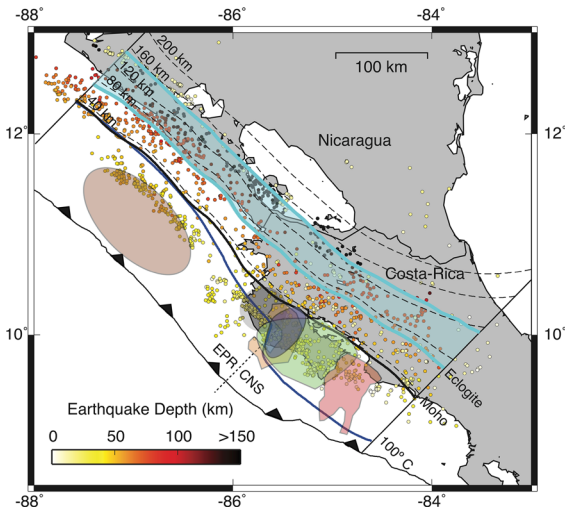


Figure 10

Map of the modeling area, with earthquake locations obtained by the TUCAN (ABERS *et al.* 2004) and CRSEIZE (http://es.ucsc.edu/~hdeshon/crseize_homepage.html) deployments. The 100 °C isotherm for the slab surface is shown in dark blue. The range over which the entire oceanic crust transforms to eclogite is shown in light blue. The intersection of the slab surface with the upper plate (Caribbean) Moho is shown in black. Slab depth contours are shown with dashed black lines. Approximate rupture areas for the 1900 (black Mw 7.2), 1950 (green Mw 7.7), 1978 (blue Mw 6.9), 1990 (red Mw 7.0), and 2012 (orange Mw 7.6) Nicoya megathrust earthquakes (YUE *et al.* 2013; PROTTO *et al.* 2014), as well as the 1992 (brown Mw 7.7) Nicaragua earthquake (KANAMORI and KIKUCHI 1993) are shown. The dotted line divides East Pacific Rise (EPR) and Cocos-Nazca Spreading Centre (CNS) lithospheres

the predicted seismogenic zone starts at 20–30 km from the trench and terminates at 70 km from the trench. In contrast, a seismogenic zone width of 20–30 km is predicted for the southeastern EPR segment, starting at 70–80 km from the trench. The width of the predicted seismogenic zone then decreases dramatically to a width of 10 km or less close to the border of Costa Rica with Nicaragua, and remains like that further northwest along the margin.

Figure 10 also shows rupture areas for several historical megathrust earthquakes in the Nicoya region (YUE *et al.* 2013; PROTTO *et al.* 2014). Each rupture area is roughly constrained by our model-predicted megathrust seismogenic zone. Of particular importance is the reduction in width of the predicted seismogenic zone in northern Nicoya, which correlates well with the reduction in rupture area for the 1900 (black), 1999 (blue) and 2012 (orange) Nicoya earthquakes. Further north, however, our results do

not fit the inferred rupture area of the 1992 Nicaragua earthquake (KANAMORI and KIKUCHI 1993; WANG *et al.* 2015). Our model predicts a cool subduction interface, such that the critical temperature for the updip limit of the seismogenic zone is not reached until a depth of ~35 km. This could indicate that our chosen geotherm for the north EPR section is too cold. We also note that the published depth of this earthquake is 45 km, which places it well below the subduction interface (KIKUCHI and KANAMORI 1995), indicating that this earthquake may not have occurred on the plate interface.

In general, the predicted megathrust seismogenic zone in our 3D models is in good agreement with that of previous 2D thermal models for this region (HARRIS *et al.* 2010b), as well as other studies of the megathrust seismogenic zone that rely on more direct methods, such as earthquake locations and GPS observations (NEWMAN *et al.* 2002; DESHON *et al.* 2006; SCHWARTZ and DESHON 2007). It should be noted that the temperatures of the shallow plate interface are primarily determined by the thermal structure of the oceanic plate at the trench, as well as its geometry and convergence rate; mantle wedge flow does not significantly affect the shallow interface temperatures. The good agreement between our 3D models and previous 2D models suggests that along-margin heat transport is negligible for the shallow subduction interface. As shown in Fig. 10, the transition in the location of the 100 °C isotherm between the EPR and CNS segments occurs over an along-strike width of less than 30 km, suggesting that 2D models are suitable for modeling interface temperatures for much of this subduction zone.

4.2. Slab Temperatures and Eclogitization of the Cocos Plate

The width of the megathrust seismogenic zone is controlled by the temperature along the interface between the oceanic plate and the overriding plate. For deeper sections within the plate, temperature also regulates the depth of release of water stored in the plate and the distribution of intraslab earthquakes (KIRBY *et al.* 1996). As the Cocos plate subducts, it is progressively being exposed to greater pressures and temperatures, causing it to undergo several

metamorphic and dehydration reactions. The main components of the oceanic crust and mantle lithosphere are mid-ocean ridge basalt (MORB) and harzburgite, respectively (IRIFUNE 1993). For the case of the oceanic crust, the MORB eventually transforms to eclogite. This process dehydrates the slab and significantly increases its density. For the oceanic mantle lithosphere, hydration of harzburgite leads to serpentization of the mantle. Serpentinite is usually stable until depths of 60–70 km for most subduction zones (SCHMIDT and POLI 2003). At larger depths, serpentinite starts to dehydrate. In general, water trapped in serpentized harzburgite may be the most efficient transport mechanism of water to the deep mantle (RÜPKE *et al.* 2004). For this study, however, we only investigated the 3D temperature distribution within the oceanic crust. A full discussion of lithosphere mantle temperatures and dehydration is given in ROSAS *et al.* (2015, submitted).

Figure 9 shows the PT paths of the top of the Cocos plate superimposed on a phase diagram for MORB (HACKER *et al.* 2003). The PT paths show minimal variations between 3D and 2D models at shallow depths. For all 4 profiles, the surface of the slab goes through the jadeite lawsonite blueschist (JLB) and lawsonite amphibole eclogite (LAE) facies, before entering the amphibole eclogite (AE) facies at 70–75 km depth. At this point, the oceanic crust is almost dry, with less than 2 wt% H₂O. At greater depths, differences between 3D and 2D models are larger due to along-strike flow. For profile A, the difference between 3D and 2D models steadily increases with depth. At a depth of 180 km, the difference is 80–90 °C. For profiles B, C and D, the difference is much less (10–20 °C).

Figure 10 shows a map view of the predicted location of the transition to eclogite (light blue) in the oceanic crust for our 3D model, assuming no kinetic delay. The seaward boundary of the region represents the point at which the top of the slab transforms to eclogite (Fig. 9), whereas the landward boundary represents the point at which the entire oceanic crust (assumed to have a thickness of 7 km) is predicted to undergo complete eclogitization. The depth for complete eclogitization of the oceanic crust ranges between 120 and 160 km along our modeling area. The predicted phase change can be compared to the

location of intraslab earthquakes. Earthquake locations were obtained from the TUCAN seismic experiment (ABERS *et al.* 2004) and UCSC-CRSEI-ZEA data archive (http://es.ucsc.edu/~hdeshon/crseize_homepage.html). Figure 6c shows the location of intraslab earthquakes along Profiles A and D. For these profiles, earthquakes in the oceanic crust are absent at depths of >90–100 and >170 km, respectively, consistent with the predicted range for eclogitization of our 3D model.

4.3. Mantle Wedge Temperatures and Flow Field

Mantle wedge temperatures are important for the generation of melt and arc volcanism. Depending in the amount of water in the mantle wedge, temperatures of 1100–1300 °C are needed for melting (SCHMIDT and POLI 1998). Figure 11 shows the geotherms along a vertical line located at a point where the slab reaches a depth of 100 km, consistent with the global average location of the volcanic arc

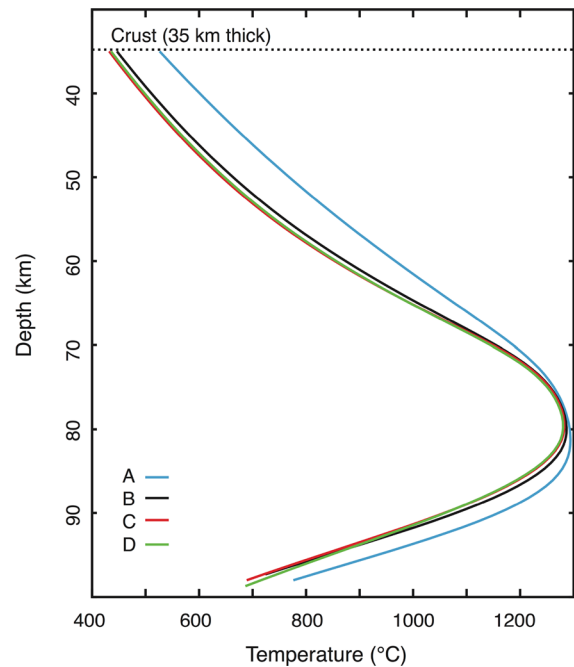


Figure 11
Volcanic arc geotherms for profiles A through D for our 3D thermal model. Geotherms were taken along a vertical line located at a point where the slab reaches a depth of 100 km (see Fig. 6c for profiles A and C). Thin dashed line shows the Moho of the continental crust

(SYRACUSE and ABERS 2006). For profile A, temperatures are up to 100 °C higher than for the other profiles. As shown in Fig. 8, 3D modeling predicts larger temperatures than 2D modeling (up to 40 °C) below the volcanic arc for this profile. It is unclear how this will affect melt production and arc volcanism, as melting also depends on the water content (SCHMIDT and POLI 1998). Assuming a similar water content for the mantle wedge along the strike, the higher temperatures observed below Costa Rica would suggest more melting in this region than for Nicaragua. However, seismic studies near the trench show that the incoming Cocos plate might carry large amounts of water along its Nicaraguan section, where significant fracturing occurs in the outer rise prior to subduction (ABERS *et al.* 2003; SYRACUSE *et al.* 2008; RYCHERT *et al.* 2008; Van AVENDONK *et al.* 2011; DINC *et al.* 2011). Thus, the Cocos plate may release more water into the wedge below Nicaragua than for Costa Rica, which can significantly affect the generation of melt.

As discussed in Sect. 3.1, an important result from our 3D models is that the observed along-strike changes in the slab geometry can induce along-strike mantle flow of up to 4 cm/year (Fig. 4b). In our models, significant along-strike flow toward the southeast is predicted below Costa Rica. This flow is driven by the southward decrease in dip angle of the subducting plate. In contrast, geochemical and seismic studies indicate a northward lateral flow, with a magnitude of 6–19 cm/year (HOERNLE *et al.* 2008). Our models show that such flow is not driven by along-strike changes in slab dip and trench curvature. If these observations are correct, an additional driving mechanism for along-strike flow must be considered. One possibility is mantle flow through the slab window just to the southeast of the study area (Fig. 1). Such flow may be enhanced by rollback of the Cocos plate as it subducts. Given that our moderate along-strike flow can increase temperatures by up to 40 °C in the mantle wedge (Figs. 8, 11) and by 80–90 °C along the slab at depths >180 km (Fig. 9) along profile A, we expect the 6–19 cm/year flow predicted by geochemical studies to have an even larger effect on mantle and slab temperatures. We are currently working on numerical models that

incorporate this flow to assess its effect in the thermal structure of the subduction zone.

5. Conclusions

Previous 3D thermal modeling studies of subduction zones investigated the relation between flow and anisotropy (KNELLER and van KEKEN 2008) or the effects of obliquity and trench curvature on slab surface temperatures (BENGTON and van KEKEN 2012). However, these studies do not discuss the thermal structure of the wedge in detail. WADA *et al.* (2015) presented a 3D thermal model for the subduction zone of northeast Japan and found that the obliquity of the trench generates an along-strike flow component that results in a different thermal structure than for a 2D corner flow model. In our study, we present the first 3D model of the Costa Rica-Nicaragua subduction zone.

The key conclusions of this work are:

1. Velocity field for the mantle:

Variations in the slab dip in the Costa Rica-Nicaragua subduction zone lead to along-strike mantle flow, with a maximum magnitude of 2.5 cm/year for an isoviscous wedge and 4 cm/year for a wedge that deforms through dislocation creep (approximately 40 % of the slab convergence rate). The predicted flow direction is toward the southeast, in the direction of decreasing slab dip. This is opposite to the flow direction inferred from geochemical and seismic observations (HOERNLE *et al.* 2008), which suggests that an additional mechanism to create along-margin flow is needed for this subduction zone. Just south of our modeling area, there appears to be a slab window that is created by the subduction of the Cocos-Nazca spreading centre (JOHNSTON and THORKELSON 1997; ABRATIS and WORNER 2001). Future 3D models should investigate how this may affect the mantle wedge flow field, especially below Costa Rica.

2. Thermal effects of 3D mantle flow:

The thermal structure of the subduction zone depends on the rheology of the mantle wedge. In addition, along-strike flow can change the

temperature of the mantle wedge. In our 3D models, we find that along-strike flow of an isoviscous wedge results in cooler temperatures below the volcanic arc with respect to the corresponding 2D model. A dislocation creep rheology has the opposite effect: higher along-strike flow velocities lead to a hotter 3D model. The temperature differences between 2D and 3D are up to 50 °C and are largest below central Costa Rica (profile A), where along-strike flow has the highest magnitude. Given that dislocation creep is considered the primary mechanism for mantle wedge deformation and that dislocation creep has the opposite effect on temperatures than the isoviscous case, we conclude that 3D isoviscous are probably not well suited for studies of 3D subduction zone thermal structure.

3. Slab temperatures in Costa Rica-Nicaragua:

The temperatures of the shallow subducting plate (<35 km depth) are not significantly altered by 3D effects. Our predicted megathrust seismogenic zone correlates well with that obtained in other 2D modeling studies (HARRIS *et al.* 2010b) in the vicinity of the Nicoya peninsula. It also matches rupture areas of historical earthquakes in this area. For the Nicaragua section, our model suggests a very narrow seismogenic zone (<10 km wide). This does not fit the observed rupture area of the 1992 earthquake (Fig. 9), and this discrepancy needs to be explored in more detail. For the deeper parts of the slab, temperatures are affected by mantle wedge flow, resulting in difference of up to 80–90 °C between 2D and 3D modeling. This can affect factors such as eclogitization and dehydration of the subducting oceanic plate, as well as the stability of serpentinized mantle within the subducting mantle.

4. Applicability of two-dimensional models to the Costa Rica-Nicaragua Subduction Zone:

Our 3D models show that changes in slab dip lead to along-strike flow up to 4 cm/year, which results in temperature variations up to 50 °C for the subducting oceanic plate and mantle wedge compared to 2D models. This variation may have implications for metamorphism and dehydration of the deep slab and mantle wedge melting. In addition, if the significant along-strike flow

(6–19 cm/year) from geochemical and seismic studies (HOERNLE *et al.* 2008) is correct, it is reasonable to expect thermal changes that are much larger than those observed in our study. This indicates that 2D models are not suitable for modeling the thermal structure of the Costa Rica-Nicaragua subduction zone at mantle depths, as they are unable to capture all the complexity of mantle wedge dynamics.

6. Appendix: Effect of side boundary conditions on mantle wedge flow

In Sect. 2, the side boundaries of the model domain are described as free-slip, insulated boundaries. This no-flow condition ($v_x = 0$) forces the mantle to follow a 2D corner flow pattern near the side boundaries. In 3D models, along-strike flow can result from along-strike changes in the dip, trench curvature, or obliquity in convergence direction relative to the trench. Thus, it is clear that the side boundary conditions become important, and may adversely affect the model results if there are any of these geometrical factors near the boundaries, as the $v_x = 0$ restriction would act to inhibit any along-strike flow.

For our Costa Rica-Nicaragua model, profiles A and D are the closest ones to the southeast and northwest boundaries, respectively. For profile A, the dip at depths of ~40 km changes from ~70° below northern Costa Rica to ~45° in central and southern Costa Rica. The thermal changes between 3D and 2D models observed in Figs. 8 and 9 result from this change in slab dip. However, the distance of this profile to the side boundary is 50 km, which means that the effect of the no-flow boundary condition described above could affect the along-strike component of mantle flow and the resulting temperature distribution.

To assess the effects of the side boundary, we have tested an additional model in which the along-strike model width is increased by 250 km. Figure 12 shows the top view of the extended 3D model, with the original boundaries indicated. In the extended model, the southern boundary is 150 km south of the

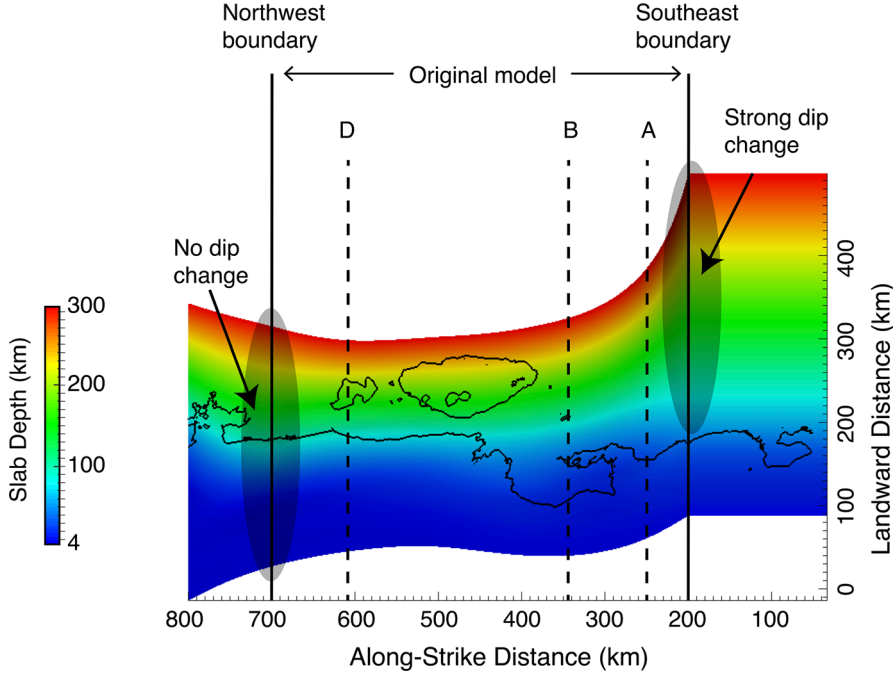


Figure 12

Slab geometry of the 3D extended model. *Color scale* denotes the depth of the slab. *Solid black lines* are the original model boundaries; *dashed lines* the location of the profiles A, B and D. Profile C is omitted, as it is located far away from the boundaries. In the extended model, the southeast boundary is located 150 km further south of that in the original model, assuming a constant slab geometry. For the northwest boundary, the extended model is 100 km further south of the original model boundary and the slab geometry is taken from KYRIAKOPOULOS *et al.* (2015). Black circle in the vicinity of the southern boundary shows the location of a strong along-strike dip gradient. For the northwest boundary, no significant dip gradient is observed

original model boundary. To assign the slab geometry in the new region, there are two possibilities. First, the slab geometry from KYRIAKOPOULOS *et al.* (2015) could be used (Fig. 1). However, the data show a significant decrease in dip south of the original model area, with a slab that is imaged to a maximum depth of ~ 75 km at the southern limit of the KYRIAKOPOULOS *et al.* (2015) study. This is a problem because of the maximum slab depth of 300 km imposed in our models. To solve this, we could extrapolate the slab geometry to a depth of 300 km, but this would result in a considerable shift of the backarc boundary in the landward direction, resulting in a highly distorted model geometry, which may lead to further numerical artifacts. We also note a complete absence of volcanoes (Fig. 1) and slab seismicity at depths >100 km (PROTTI *et al.* 1995) in this region, which suggest that the slab geometry should not be simply extrapolated to 300 km depth.

A second possibility is to take the geometry of the south boundary and apply it to the new section of the model. This would allow along-margin flow to pass through the original model boundary and therefore reduce the effect of the no-flow boundary condition on temperatures near the boundary. However, because the extended region has a constant dip, a strong along-strike gradient in dip is generated near the location of the original boundary (black circle in Fig. 12).

Figure 13 shows the temperature difference between the original 3D model and the extended 3D model, for a mantle wedge with an isoviscous rheology. The slab geometry of the extended region is the geometry of the south boundary, as discussed in the previous paragraph. The figure also shows the along-strike flow component for profiles A and B in the extended model; the along-strike flow for these profiles in the original model is shown in Fig. 7. For

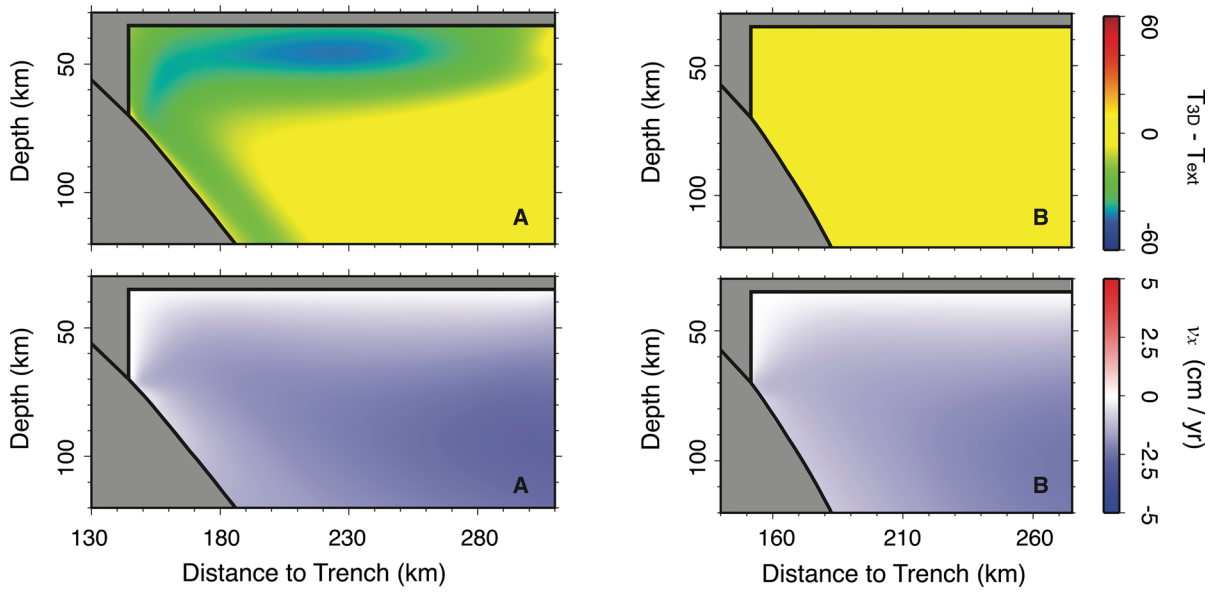


Figure 13

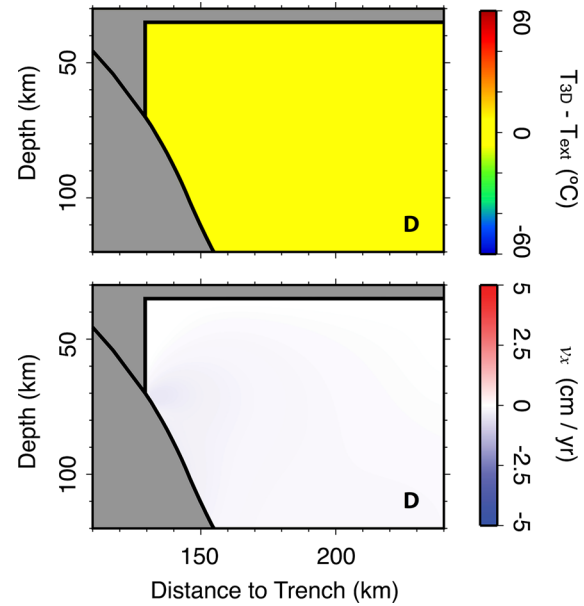
Thermal difference between the original 3D model (T_{3D}) and the extended 3D model (text), and the along-strike velocity component for the extended model, for profiles A and B

profile A, the extended model has that temperatures in the upper mantle wedge are ~ 30 to 50 °C cooler than in the original models. This appears to be related to the higher magnitude of along-strike flow that is generated in the extended model (compare Figs. 13, 7). For profile B, there is very little difference between our original model and the extended model, which indicates that the boundary condition does not influence the thermal structure at this location.

From this, we conclude that the model results for Profile A in the original models may be affected by the side boundary. However, as the geometry from the extended model is not a real feature of the Cocos plate (is merely an extension of the geometry from the south boundary of the original model), the large temperature change observed in Fig. 13 is also not a feature that would be observed in reality. We thus prefer the original model over the extended model because the former is limited to real features of the slab geometry as provided by KYRIAKOPOULOS *et al.* (2015), although we acknowledge the effect of the side boundary is important.

At the north end of the modeling area, the original side boundary is moved 100 km to the north in the extended model, and the slab geometry in this section uses the geometry from KYRIAKOPOULOS *et al.* (2015)

(Fig. 12). In the extended geometry, profile D is located 190 km away from the boundary. The along-strike variations in dip near this profile are not as large as for profile A. Figure 14 shows there are negligible differences in the thermal structure and a comparison

Figure 14
Same as Fig. 2a, but for profile D

of the along-strike velocity for this profile in Figs. 8 (original model) and 14 (extended model) shows no obvious difference. Therefore, we do not believe that there are any adverse effects from the side boundary at the north end of our original models.

Acknowledgments

We thank Christodoulos Kyriakopoulos for providing the updated geometry of the Cocos plate prior to publication, Felipe da Cruz Pimentel Moreira Santos for his technical support in creating the 2D meshes, Geoffrey Abers and Ellen Syracuse for providing earthquake locations shown in Figs. 4 and 11, and Robert Harris for discussions about hydrothermal circulation. We also thank Ikuko Wada and Vlad Manea for helpful and thoughtful reviews and William Bandy for his editorial handling of the manuscript. Research was funded by the Natural Sciences and Engineering Research Council of Canada (NSERC) and the National Council for Science and Technology of Mexico (CONACYT).

REFERENCES

- ABERS, G. A., AUGER, L., SYRACUSE, E., PLANK, T., FISCHER, K. M., RYCHERT, C., WALKER, A., PROTTI, J., GONZALEZ SALAS, V., STRAUCH, W., and PEREZ, P. (2004), Imaging the Subduction Factory Beneath Central America: The TUCAN Broadband Seismic Experiment. AGU Fall Meeting Abstracts.
- ABERS, G. A., PLANK, T., and HACKER, B. R. (2003), *The wet Nicaraguan slab*, Geophysical Research Letters. 30, 1–4.
- ABRATIS, M. and WORNER, G. (2001), *Ridge collision, slab-window formation, and the flux of Pacific asthenosphere into the Caribbean realm*, Geology. 29, 127–130.
- AUDET, P. and SCHWARTZ, S. Y. (2013), *Hydrologic control of forearc strength and seismicity in the Costa Rican subduction zone*, Nature Geoscience. 6, 852–855.
- BARCKHAUSEN, U., RANERO, C. R., HUENE, R., CANDE, S. C., and ROESER, H. A. (2001), *Revised tectonic boundaries in the Cocos plate off Costa Rica: implications for the segmentation of the convergent margin and for plate tectonic models*, Journal of Geophysical Research: Solid Earth. 106, 19207–19220.
- BATCHELOR, G. K. An introduction to fluid dynamics (Cambridge University, Cambridge, 2000).
- BENGTON, A. K. and van KEKEN, P. E. (2012), *Three-dimensional thermal structure of subduction zones: effects of obliquity and curvature*. Solid Earth. 3, 365–373.
- BILLEN, M. I. (2008), *Modeling the dynamics of subducting slabs*. Annual Review of Earth and Planetary Sciences. 36, 325–356.
- BIRD, P. (2003), *An updated digital model of plate boundaries. Geochemistry, Geophysics, Geosystems*. 4. doi:[10.1029/2001GC000252](https://doi.org/10.1029/2001GC000252).
- CARR, M. J., FEIGENSON, M. D., PATINO, L. C., and WALKER, J. A. (2004) Volcanism and geochemistry in Central America: progress and problems, In Inside the Subduction Factory (ed. EILER, J.) (American Geophysical Union, Washignton D.C. 2004) pp. 153–174.
- CLOOS, M. (1993), *Lithospheric buoyancy and collisional orogenesis: subduction of oceanic plateaus, continental margins, island arcs, spreading ridges, and seamounts*, Geological Society of America Bulletin. 105, 715–737.
- COZZENS, B. D. and SPINELLI, G. A. (2012), *A wider seismogenic zone at Cascadia due to fluid circulation in subducting oceanic crust*, Geology. 40, 899–902.
- CURRIE, C., WANG, K., HYNDMAN, R. D., and HE, J. (2004), *The thermal effects of steady-state slab-driven mantle flow above a subducting plate: the Cascadia subduction zone and backarc*, Earth and Planetary Science Letters. 223, 35–48.
- CURRIE, C. A. and HYNDMAN, R. D. (2006), *The thermal structure of subduction zone back arcs*. Journal of Geophysical Research. 111. doi:[10.1029/2005JB004024](https://doi.org/10.1029/2005JB004024).
- DAVIS, E. E., WANG, K., HE, J., CHAPMAN, D. S., VILLINGER, H., and ROSENBERGER, A. (1997), *An unequivocal case for high Nusselt number hydrothermal convection in sediment-buried igneous oceanic crust*, Earth and Planetary Science Letters. 146, 137–150.
- DEMETS, C. (2001), *A new estimate for present-day Cocos-Caribbean plate motion: implications for slip along the Central American volcanic arc*, Geophysical Research Letters. 28, 4043–4046.
- DESHON, H. R., SCHWARTZ, S. Y., NEWMAN, A. V., GONZALEZ, V., PROTTI, M., DORMAN, L. M., DIXON, T. H., SAMPSON, D. E., and FLUEH, E. R. (2006), *Seismogenic zone structure beneath the Nicoya peninsula, Costa Rica, from three-dimensional local earthquake P- and S-wave tomography*, Geophysical Journal International. 164:109–124.
- DINC, A. N., RABELL, W., FLUEH, E. R., and TAYLOR, W. (2011). *Mantle wedge hydration in Nicaragua from local earthquake tomography*, Geophysical Journal International. 186, 99–112.
- FISHER, A. T., STEIN, C. A., HARRIS, R. N., WANG, K., SILVER, E. A., PFENDER, M., HUTNAK, M., CHERKAUI, A., BODZIN, R., and VILLINGER, H. (2003), *Abrupt thermal transition reveals hydrothermal boundary and role of seamounts within the Cocos plate*, Geophysical Research Letters. 30. doi:[10.1029/2002GL016766](https://doi.org/10.1029/2002GL016766).
- FORSYTH, D. and UYEDA, S. (1975), *On the relative importance of the driving forces of plate motion*, Geophysical Journal of the Royal Astronomical Society. 43, 163–200.
- HACKER, B. R., ABERS, G. A., and PEACOCK, S. M. (2003), *Subduction factory 1. Theoretical mineralogy, densities, seismic wave speeds, and H₂O contents*, Journal of Geophysical Research. 108. doi:[10.1029/2001JB001127](https://doi.org/10.1029/2001JB001127).
- HARRIS, R. N., GREVEMEYER, I., RANERO, C. R., VILLINGER, H., BARCKHAUSEN, U., HENKE, T., MUELLER, C., and NEBEN, S. (2010a), *Thermal regime of the Costa Rican convergent margin: 1. Along-strike variations in heat flow from probe measurements and estimated from bottom-simulating reflectors*, Geochemistry, Geophysics, Geosystems. 11. doi:[10.1029/2010GC003272](https://doi.org/10.1029/2010GC003272).
- HARRIS, R. N., SPINELLI, G., RANERO, C., GREVEMEYER, I., VILLINGER, H., and BARCKHAUSEN, U. (2010b), *Thermal regime of the Costa Rican convergent margin: 2. Thermal models of the shallow Middle America subduction zone offshore Costa Rica*, Geochemistry, Geophysics, Geosystems. 11. doi:[10.1029/2010GC003273](https://doi.org/10.1029/2010GC003273).

- HARRIS, R. N. and WANG, K. (2002), *Thermal models of the Middle America trench at the Nicoya peninsula, Costa Rica*, Geophysical Research Letters. 29, 1–4.
- HERRSTROM, E. A., REAGAN, M. K., and MORRIS, J. D. (1995), *Variations in lava composition associated with flow of asthenosphere beneath southern Central America*, Geology. 23, 617–620.
- HOERNLE, K., ABT, D. L., FISCHER, K. M., NICHOLS, H., HAUFF, F., ABERS, G. A., van den BOGAARD, P., HEYDOLPH, K., ALVARADO, G., PROTTO, M., and STRAUCH, W. (2008), *Arc-parallel flow in the mantle wedge beneath Costa Rica and Nicaragua*, Nature. 451, 1094–1097.
- HUTNAK, M., FISHER, A. T., HARRIS, R., STEIN, C., WANG, K., SPINELLI, G., SCHINDLER, M., VILLINGER, H., and SILVER, E. (2008), *Large heat and fluid fluxes driven through mid-plate outcrops on ocean crust*, Nature Geoscience. 1, 611–614.
- HYNDMAN, R.D., YAMANO, M., OLESKEVICH, D.A. (1997), *The seismogenic zone of subduction thrust faults*, Island Arc. 6, 244–260.
- IRIFUNE, T. (1993), *Phase transformations in the earth's mantle and subducting slabs: implications for their compositions, seismic velocity and density structures and dynamics*, Island Arc. 2, 55–71.
- JOHNSTON, S. T. and THORKELSON, D. J. (1997), *Cocos-Nazca slab window beneath Central America*, Earth and Planetary Science Letters. 146, 465–474.
- GANAMORI, H. and KIKUCHI, M. (1993), *The 1992 Nicargua earthquake: a slow tsunami earthquake associated with subducted sediments*, Nature. 361, 714–716.
- KARATO, S.-i. and WU, P. (1993), *Rheology of the upper mantle: a synthesis*, Science. 260, 771–778.
- KIKUCHI, M. and KANAMORI, H. (1995), *Source characteristics of the 1992 Nicargua tsunami earthquake inferred from teleseismic body waves*, Pure and Applied Geophysics. 144, 441–453.
- KIRBY, S., ENGDAHL, R.E., DENLINGER, R. (1996), Intermediate-depth intraslab earthquakes and arc volcanism as physical expressions of crustal and uppermost mantle metamorphism in subducting slabs, in Subduction Top to Bottom (ed. BEBOUT, G., SCHOLL, D., KIRBY, S., PLATT, J.) (American Geophysical Union, Washignton D.C 1996) pp. 195–214.
- KNELLER, E. A. and van KEKEN, P. E. (2008), *Effect of three-dimensional slab geometry on deformation in the mantle wedge: implications for shear wave anisotropy*, Geochemistry, Geophysics, Geosystems. 9. doi:[10.1029/2007GC001677](https://doi.org/10.1029/2007GC001677).
- KYRIAKOPOULOS, C., NEWMAN, A.V., THOMAS, A.M., MOORE-DRISKELL, M., FARMER, G.T. (2015), *A new seismically constrained subduction interface model for Central America*, Journal of Geophysical Research. 120, 5535–5548.
- KUMMER, T. and SPINELLI, G. A. (2008), *Hydrothermal circulation in subducting crust reduces subduction zone temperatures*, Geology. 36, 91–94.
- LANGSETH, M. G. and SILVER, E. A. (1996), *The Nicoya convergent margin—a region of exceptionally low heat flow*, Geophysical Research Letters. 23, 891–894.
- LONG, M. D. and SILVER, P. G. (2008), *The subduction zone flow field from seismic anisotropy: a global view*, Science. 319, 315–8.
- MACKENZIE, L. S., ABERS, G. A., FISCHER, K. M., SYRACUSE, E. M., PROTTO-QUESADA, J. M., GONZÁLEZ-SALAS, V., and STRAUCH, W. (2008), *Crustal structure along the southern Central American volcanic front*, Geochemistry, Geophysics, Geosystems. 9. doi:[10.1029/2008GC001991](https://doi.org/10.1029/2008GC001991).
- MANEA, VLAD C., MANEA, M., KOSTOGLODOV, V., SEWELL, G. (2005), *Thermo-mechanical model of the mantle wedge in Central Mexican subduction zone and a blob tracing approach for the magma transport*, Physics of the Earth and Planetary Interiors. 149, 165–186.
- MANEA, VLAD C. and GURNIS, M. (2007), *Subduction zone evolution and low viscosity wedges and channels*, Earth and Planetary Science Letters. 264, 22–45.
- MANEA, M. and MANEA, VLAD C. (2008), *On the origin of El Chichón volcano and subduction of Tehuantepec Ridge: a geodynamical perspective*, Journal of Volcanology and Geothermal Research. 175: 459–471.
- MANEA, VLAD C., MANEA, M., FERRARI, L. (2013), *A geodynamical perspective on the subduction of Cocos and Rivera plates beneath Mexico and Central America*, Tectonophysics. 609, 56–81.
- NEWMAN, A. V., SCHWARTZ, S. Y., GONZALEZ, V., DESHON, H. R., PROTTO, J. M., and DORMAN, L. M. (2002), *Along-strike variability in the seismogenic zone below Nicoya peninsula, Costa Rica*, Geophysical Research Letters. 29, 1–4.
- PATINO, L. C., MICHAEL, A., CARR, J., MARK, A., and FEIGENSON, D. (2000), *Local and regional variations in Central American arc lavas controlled by variations in subducted sediment input*, Contributions to Mineralogy and Petrology. 2000, 265–283.
- PEACOCK, S., van KEKEN, P., HOLLOWAY, S., HACKER, B., ABERS, G. A., and FERGASON, R. (2005), *Thermal structure of the Costa Rica-Nicaragua subduction zone*, Physics of the Earth and Planetary Interiors. 149, 187–200.
- PEACOCK, S. M. (1996), Thermal and petrologic structure of subduction zones, in subduction top to bottom (ed. BEBOUT, G., SCHOLL, D., KIRBY, S., PLATT, J.) (American Geophysical Union, Washington D.C 1996) pp. 119–133.
- PROTTI, M., GUENDEL, F., McNALLY, K. (1995), *Correlation between the age of the subducting Cocos plate and the geometry of the Wadati-Benioff zone under Nicargua and Costa Rica*, Geological Society of America Special Papers. 295, 309–326.
- PROTTI, M., GONZALEZ, V., NEWMAN, A. V., DIXON, T. H., SCHWARTZ, S. Y., MARSHALL, J. S., FENG, L., WALTER, J. I., MALSERVISI, R., and OWEN, S. E. (2014), *Nicoya earthquake rupture anticipated by geodetic measurement of the locked plate interface*, Nature Geoscience. 7, 117–121.
- ROSAS, J.C., CURRIE, C., HARRIS, R., HE, J. (2015), *Effect of hydrothermal circulation on slab dehydration for the subduction zone of Costa Rica and Nicargua*, Physics of the Earth and Planetary Interiors. Submitted.
- ROTMAN, H. M. M. and SPINELLI, G. A. (2013), *Global analysis of the effect of fluid flow on subduction zone temperatures*, Geochemistry, Geophysics, Geosystems. 14, 3268–3281.
- RYCHERT, C. A., FISCHER, K. M., ABERS, G. A., PLANK, T., SYRACUSE, E., PROTTO, J. M., GONZALEZ, V., and STRAUCH, W. (2008), *Strong along-arc variations in attenuation in the mantle wedge beneath Costa Rica and Nicaragua*, Geochemistry, Geophysics, Geosystems. 9. doi:[10.1029/2008GC002040](https://doi.org/10.1029/2008GC002040).
- RÜPK, L., MORGAN, J., HORTH, M., CONNOLLY, J. (2004), *Serpentine and the subduction zone water cycle*, Earth and Planetary Science Letters. 223, 17–34.
- SCHMIDT, M. W. and POLI, S. (1998), *Experimentally based water budgets for dehydrating slabs and consequences for arc magma generation*, Earth and Planetary Science Letters. 163, 361–379.
- SCHMIDT, M. W. and POLI, S. (2003), *Generation of mobile components during subduction of Oceanic Crust*, in Treatise on

- Geochemistry (ed. RUDNICK, R., HOLLAND, H.D., TUREKIAN, K.K.) (Elsevier, 1996) pp. 567–591.
- SCHWARTZ, S. Y. and DESHON, H. R. (2007), Distinct geodetic and seismic up-dip limits to the northern Costa Rica seismogenic zone: evidence for two mechanical transitions, in *The Seismogenic Zone of Subduction Thrust Faults* (ed. DIXON, T., MORE, J.) (Columbia University Press, New York 2007) pp. 576–599.
- SOTO, G. L., NI, J. F., GRAND, S. P., SANDOVOL, E., VALENZUELA, R. W., SPEZIALE, M. G., GONZÁLEZ, J. M. G., and REYES, T. D. (2009), *Mantle flow in the Rivera-Cocos subduction zone*, *Geophysical Journal International*. 179, 1004–1012.
- STEIN, C. and STEIN, S. (1992), *A model for the global variation in oceanic depth and heat flow with lithospheric age*, *Nature*. 359, 123–129.
- STERN, R. J. (2002), *Subduction zones*, *Reviews of Geophysics*. 40, 1–38.
- SYRACUSE, E. M., ABERS, G. A., FISCHER, K., MACKENZIE, L., RYCHERT, C., PROTTI, M., GONZALEZ, V., and STRAUCH, W. (2008), *Seismic tomography and earthquake locations in the Nicaraguan and Costa Rican upper mantle*, *Geochemistry, Geophysics, Geosystems*. 9. doi:[10.1029/2008GC001963](https://doi.org/10.1029/2008GC001963).
- SYRACUSE, E. M. and ABERS, G. A (2006), *Global compilation of variations in slab depth beneath arc volcanoes and implications*, *Geochemistry, Geophysics, Geosystems*. 7. doi:[10.1029/2005GC001045](https://doi.org/10.1029/2005GC001045).
- TURCOTTE, D. L. and SCHUBERT, G., *Geodynamics* (Cambridge University Press, Cambridge, 2002).
- Van AVENDONK, H. J. A., HOLBROOK, W. S., LIZARRALDE, D., and DENYER, P. (2011), *Structure and serpentinization of the subducting Cocos plate offshore Nicaragua and Costa Rica*, *Geochemistry, Geophysics, Geosystems*. 12. doi:[10.1029/2011GC003592](https://doi.org/10.1029/2011GC003592).
- van KEKEN, P. E., CURRIE, C., KING, S. D., BEHN, M. D., CAGNIONCLE, A., HE, J., KATZ, R. F., LIN, S.-C., PARMENTIER, E. M., SPIEGELMAN, M., and WANG, K. (2008), *A community benchmark for subduction zone modeling*, *Physics of the Earth and Planetary Interiors*. 171, 187–197.
- van KEKEN, P. E., KIEFER, B., and PEACOCK, S. M. (2002), *High-resolution models of subduction zones: implications for mineral dehydration reactions and the transport of water into the deep mantle*, *Geochemistry, Geophysics, Geosystems*. 3. doi:[10.1029/2001GC000256](https://doi.org/10.1029/2001GC000256).
- von HUENE, R., RANERO, C.R., WEINREBE, W. (2000), *Quaternary convergent margin tectonics of Costa Rica, segmentation of the Cocos plate, and Central American volcanism*, *Tectonics*. 19-314-334.
- WADA, I. and WANG, K. (2009), *Common depth of slab-mantle decoupling: reconciling diversity and uniformity of subduction zones*, *Geochemistry, Geophysics, Geosystems*. 10. doi:[10.1029/2009GC002570](https://doi.org/10.1029/2009GC002570).
- WADA, I., WANG, K., HE, J., and HYNDMAN, R. D. (2008), *Weakening of the subduction interface and its effects on surface heat flow, slab dehydration, and mantle wedge serpentinization*, *Journal of Geophysical Research*. 113. doi:[10.1029/2007JB005190](https://doi.org/10.1029/2007JB005190).
- WADA, I., J. HE, A. HASEGAWA, and J. NAKAJIMA (2015), *Mantle wedge flow pattern and thermal structure in northeast Japan: effects of oblique subduction and 3-D slab geometry*, *Earth and Planetary Science Letters*. 426, 76–88.
- WANG, K., HE, J., SCHULZECK, F., HYNDMAN, R. D., and RIEDEL, M. (2015). *Thermal condition of the 27 October 2012 Mw 7.8 Haida Gwaii subduction earthquake at the obliquely convergent Queen Charlotte margin*, *Bulletin of the Seismological Society of America*. 115. doi:[10.1785/0120140183](https://doi.org/10.1785/0120140183).
- YUE, H., LAY, T., SCHWARTZ, S. Y., RIVERA, L., PROTTI, M., DIXON, T. H., OWEN, S., and NEWMAN, A. V. (2013), *The 5 September 2012 Nicoya, Costa Rica Mw 7.6 earthquake rupture process from joint inversion of high-rate GPS, strong-motion, and teleseismic P-wave data and its relationship to adjacent plate boundary interface properties*, *Journal of Geophysical Research*. 118, 5453–5466.

(Received July 1, 2015, revised October 9, 2015, accepted October 13, 2015)